B- AND A-TYPE STARS IN THE TAURUS-AURIGA STAR FORMING REGION

KUNAL MOOLEY[1], LYNNE HILLENBRAND[1], LUISA REBULL[2], DEBORAH PADGETT [2,4], AND GILLIAN KNAPP[3]
[1]Department of Astronomy, California Institute of Technology, 1200 E. California Blvd., MC 249-17, Pasadena, CA 91125, USA; kunal@astro.caltech.edu
[2]Spitzer Science Center, California Institute of Technology, Pasadena, CA 91125, USA
[3]Department of Astrophysics, Princeton University, Princeton, NJ, USA and
[4]current address: Goddard Space Flight Center, Greenbelt, MD, USA
Draft of February 28, 2013

ABSTRACT

We describe the results of a search for early-type stars associated with the Taurus-Auriga molecular cloud complex, a diffuse nearby star-forming region typically noted as lacking young stars of intermediate and high mass. We investigate several sets of possible O, B and early A spectral class members. The first set is a group of stars for which mid-infrared images show bright nebulae, all of which can be associated with stars of spectral type B. We model the scattered and emitted radiation from the reflection nebulosity and compare the results with the observed spectral energy distributions to test the plausibility of association of the B stars with the cloud. The second group of candidates investigated consists of early-type stars compiled from (i) literature listings in SIMBAD; (ii) B stars with infrared excesses selected from the *Spitzer Space Telescope* survey of the Taurus cloud; (iii) magnitude- and color-selected point sources from the *Two Micron All Sky Survey*; and (iv) spectroscopically identified early-type stars from the *Sloan Digital Sky Survey* coverage of the Taurus region. We evaluated stars in these categories for membership in the Taurus-Auriga star formation region based on criteria involving: spectroscopic and parallactic distances, proper motions and radial velocities, and infrared excesses or line emission indicative of stellar youth. This investigation newly identifies as probable Taurus members three B-type stars: HR 1445 (HD 28929), τ Tau (HD 29763), 72 Tau (HD 28149), and two A-type stars: HD 31305 and HD 26212. Several additional sources meet some, but not all, of the membership criteria and are plausible, though not secure, members.

Subject headings: stars: early-type, stars: Herbig Ae/Be, stars: formation, ISM: clouds

1. INTRODUCTION

The Taurus-Auriga molecular cloud complex (hereafter "Taurus") is the quintessential region of nearby recent star formation. It is characterized by low star-formation efficiency (Goldsmith et al. 2008) and the absence of high-mass young stars (Kenyon et al. 2008) and it stands in contrast to more distant, massive, and dense star-forming environments like the Orion Molecular Clouds. Taurus lies at a mean distance of about 140 pc with a depth of 20 pc or more (Kenyon et al. 1994; Torres et al. 2007, 2012) and spans approximately 100 square degrees on the sky, or about a 25 pc diameter at this distance. The cloud currently has about 350 known members, mainly low-mass stars with $M < 0.5\ M_{\odot}$, and only about 10 members identified with $M > 1.5\ M_{\odot}$. Much effort over the past decade in Taurus has been directed towards completely defining the low-mass stellar and sub-stellar population.

A comprehensive review of Taurus is given by Kenyon et al. (2008). Major recent contributions to our knowledge include: (i) mapping of the molecular gas (Goldsmith et al. 2008; Narayanan et al. 2008) and dust (Lombardi et al. 2010; Palmeirim et al. 2013) comprising the cloud; (ii) determination of the distance of individual young star members, through Very Long Baseline Interferometry (VLBI; Torres et al. 2009) parallaxes; (iii) improvement of the young stellar object census including new stellar and brown dwarf members (Rebull et al. 2010; Luhman et al. 2009, 2010; Takita et al. 2010; Rebull et al. 2011) as well as new companions to known objects (Kraus et al. 2011); (iv) measurement of proper motions using optical and VLBI techniques, (Torres et al. 2009; Luhman et al. 2009); (v) provision of evidence for mass segregation (Kirk & Myers 2011; Parker et al. 2011); and (vi) searches for outflows (Narayanan et al. 2012; Bally et al. 2012).

In particular, a *Spitzer* program directed at Taurus (Güdel et al. 2007; Rebull et al. 2010, PI D. Padgett) produced large-scale multi-wavelength maps of the clouds. Photometry from this survey has improved our understanding of both the stellar/sub-stellar membership and the incidence of protoplanetary disks. Motivating the investigation described in this paper are four large and two smaller / weaker reflected and/or scattered-light nebulae found in these mid- and far-infrared images, shown in Figure 1.

Each of the large nebulae is illuminated by a point source. Three of these sources (HD 282276, HD 28149 = 72 Tau, and HD 29647) are known B stars which, in the literature to date, have been assumed to be background stars and have been used to study the physical and chemical properties of the molecular cloud. The fourth source (V892 Tau) is a well-known Herbig Ae/Be type member of Taurus that also illuminates an optical reflection nebula — an original defining characteristic of the Herbig Ae/Be population. The two smaller/weaker nebulae are also associated with early-type or high luminosity stars (HD 28929 = HR 1445, and IC 2087). The nebular regions for all six of these sources appear brightest at mid-to-far infrared wavelengths; optical nebulosity, when present, is weak, except in the case of IC 2087.

The proximity of these early-type stars to cloud material,

as evidenced by the mid-infrared nebulae, suggests that rather than being background stars as they have been traditionally considered, they may be heretofore unappreciated early-type members of Taurus. The association of these stars with prominent nebulosity is not, however, sufficient evidence that they are genuine members of Taurus. Instead, they could be stars of early type that are physically unassociated but fortuitously located with respect to either the Taurus molecular cloud complex itself or smaller patches of locally-enhanced density in the interstellar medium (ISM). Reminiscent of this situation is the Pleiades star cluster, which is passing through and illuminating denser-than-average ISM that is physically unassociated with the stars themselves. In this contribution, we explore the evidence for physical association.

The earliest-type already-known members of the Taurus star forming region are generally considered to be IC2087-IR (estimated at B5 based on bolometric luminosity and heavily self-embedded with a continuum-emission optical spectrum), the binary system V892 Tau (Elias 1; a B8-A6 self-embedded Herbig Ae/Be star with a near-equal brightness companion), the triple system HD 28867 (B8 $+2\times$B9.5), AB Aur (A0e, a Herbig Ae/Be star), and HD 31648 (MWC 480; A2e, another Herbig Ae/Be star). There are no associated F stars [1] and the next earliest types are HP Tau/G2 (G0) and SU Aur (G2). Notably, almost all of these earliest-type members of Taurus harbor significant amounts of circumstellar material, the HD 28867 system [2] being the exception.

While no systematic investigation for high-mass stars associated with Taurus has been performed recently, there has been historical interest in early-type stars seen towards this star-forming region. Blaauw (1956) identified Casseiopeia-Taurus (hereafter Cas-Tau) as an OB association lying between 140 and 220 pc using the convergent-point method. There was ensuing debate concerning the relationship of the young Taurus-Auriga molecular cloud to the older Cas-Tau OB association, but it has now been resolved that they are unrelated in both space and age (see below). Next in historical sequence was AB Aur, an original Herbig Ae/Be star (Herbig 1960) and then the highly veiled young stellar object IC 2087-IR (Elias 1978).

How many higher-mass stars should there be in Taurus? Using the number and distribution of the known low-mass T Tauri stars and the assumption that weak-lined T Tauri stars (WTTS) are far more numerous (as high as 10:1) than classical T Tauri stars (CTTS), Walter et al. (1988) argued from a sparse X-ray survey of Taurus with *Einstein* that there should be $\sim 10^3$ low-mass members of Taurus. The initial mass function (IMF) appropriate for young star clusters (Miller & Scalo 1979) would then also predict the existence of a few tens of B star members. The search for these B stars culminated with Walter & Boyd (1991) identifying 29 possible members of the Taurus-Auriga T association based on their spectroscopic parallaxes and proper motions. However, the large number of low-mass Taurus member stars predicted by Walter et al. (1988) were not found in the proper-motion survey by Hartmann et al. (1991), who suggested that many of the stars found in the X-ray survey by Walter et al. (1988) belong to the older and more distant Cas-Tau group, and that the assumption of a uniform distribution of T Tauri stars is not correct. While Walter & Boyd (1991) had concluded that the Tau-Aur T association was related to the Cas-Tau OB association, de Zeeuw et al. (1999) showed that these are kinematically distinct groups and rejected the Walter & Boyd (1991) stars as Cas-Tau members.

Most subsequent publications on the Taurus-Auriga stellar population have focused on the low-mass stars. However, of relevance to the present study is that Whittet et al. (2004) proposed, on the basis of extinction and dust modelling, that HD 29647 (B9III) is located within a diffuse screen surrounding the dense molecular clump TMC-1 in Taurus. Also, Rebull et al. (2010) suggested that its infrared excess and spectroscopic parallax make HD 27659 (A0–A4V) a high-quality candidate member of Taurus, and that HD 282276 (B8V) and HD 283815 (A0V) are lower-quality, but plausible, candidate members. As the situation concerning associated early-type stars remains unclear, and considering the high level of interest in the membership and star-formation history of Taurus, a detailed investigation using the wealth of new information seems warranted.

This paper is organized as follows. In §2 we describe the process of compiling the list of early-type stars towards Taurus (§2.2) and testing these stars for membership (§2.3). Our literature survey showed that spectral typing and age estimation of some of the stars was done decades ago with prism-based spectrometers, and so we considered the possibility that some known early-type stars have been assigned an incorrect spectral type. Additionally, we considered that some early-type stars could have been missed due to limits on the spatial extent or photometric depth of previous investigations. We spectroscopically followed up all probable members (§2.4). Notes on individual objects, including newly-appreciated early-type Taurus members identified here, are provided in §3. Finally, we return to the initial motivation for this investigation, that our inspection of the Spitzer mosaics of Taurus revealed reflection/scattered-light nebulae toward several known B stars. We model the scattered/thermal dust emission for several of these nebulae in §4. We conclude with a summary and discussion in §5.

2. DATA COLLECTION AND ANALYSIS

2.1. *OVERVIEW*

Working from the evidence of early-type members provided by the reflection/scattered-light nebulae and the recent suggestions of additional B and A0 type stars as plausible members, we carried out a new search for stars of spectral classes O–A0 associated with Taurus. The areal extent of our study is the region bounded by 4^h and 5^h in right ascension and 22°and 31°in declination. Equivalently, in galactic coordinates, this is roughly the region $(165, -20) \lesssim (l, b) \lesssim (180, -10)$. This boundary was chosen to include most of

[1] HD 283759 (F2–F3) and V410-Anon24 (F9–G3) have at various times been suggested as members, but both are well underluminous with respect to the other stars in this list if assumed to be at the same distance, and not particularly obscured.

[2] This source is to the south of the main Taurus-Auriga clouds and not otherwise discussed in this paper.

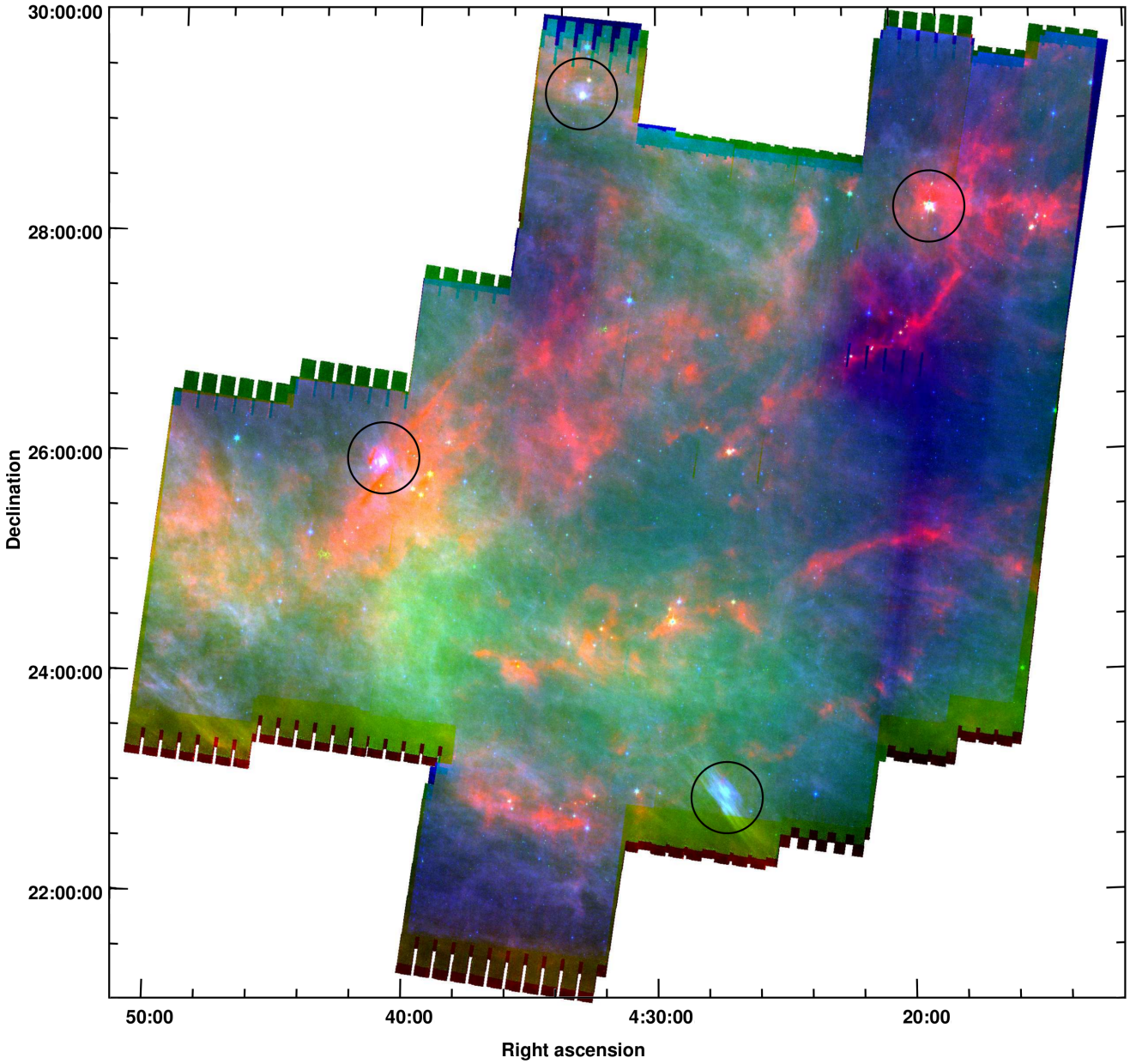

Figure 1. Spitzer mosaic of IRAC and MIPS images of Taurus. Color coding: 8 (blue), 24 (green), and 160 (red) μm. Four bright nebulous objects illuminated by B stars are evident in this mosaic. They have been marked with a circle and are associated with: (i) top-middle: HD 282276, (ii) top-right: V892 Tau (Elias 1), (iii) bottom-middle: HD 28149 (72 Tau), and (iv) middle-left: HD 29647. Two other sources, HD 28929 (HR 1445) and IC 2087, are discussed in the text as having nebulae weaker than can be seen at this image scale.

the dense cores in Taurus but not to be so large as to obfuscate the search with unassociated early-type stars at different distances. The region south of the Taurus main cloud between 4.3^h and 4.9^h in right ascension and 16°and 20°in declination is also considered a part of the Taurus star-forming region, but is not included in this investigation.

We first looked at whether there is a concentration of early-type stars towards or away from the large patch of sky under consideration. A SIMBAD query for known O,B stars towards Taurus and eight neighboring regions of equal areal extent results in the distribution shown in Table 1. There is a higher density of known early-type stars in the direction of the galactic plane as expected, and no particular bias of early-type stars at the longitude of Taurus compared to adjacent longitudes. Thus, from our study, we expect to find only a few known early-type stars, if any, that are genuinely associated with, or bona fide members of, Taurus.

In order to compile the list of candidate early-type stars towards Taurus, we gathered multiwavelength photometric and spectroscopic data and images, and collected information from the literature. We then passed these stars through two membership tests: appropriate distance and appropriate kinematics. All candidates satisfying these two criteria were labeled as probable members of Taurus. The probable members along with a few other stars of potential interest were followed up spectroscopically.

In view of the content presented below, the reader is reminded that at the Taurus distance of 140 pc, a B8 dwarf and a B8 giant star would have unreddened V-band apparent magnitudes of approximately 6.3 and 4.7, respectively. However, the reddening towards Taurus is variable and can be significant, up to 30 magnitudes through the densest molecular cores (Cernicharo & Bachiller 1984; Lombardi et al. 2010).

2.2. *COMPILING THE LIST OF CANDIDATE EARLY-TYPE STARS AND ANCILLARY DATA*

Four data sets were used to assemble a list of early-type stars towards the Taurus region: (i) previously identified O and B-type stars listed in SIMBAD; (ii) proposed B and early A stars with infrared excesses selected from the *Spitzer* survey of the Taurus cloud discussed in Rebull et al. (2010); (iii) photometrically-selected point sources from the *Two Micron All Sky Survey* (2MASS-PSC; Skrutskie et al. 2006); and (iv) spectroscopically identified early-type stars from the *S*loan Digital Sky Survey (*SDSS*) observations of the Taurus region (Finkbeiner et al. 2004) presented by Knapp et al. (2007). As illustrated in Figure 2, there is only partial coverage of the total cloud region (see also Figure 4) in each of *SDSS* and the Rebull et al. (2010) *Spitzer* surveys, and the overlap between the optical and infrared photometric surveys is also only partial.

We now describe the collation of data from each of the four sources. First, to select early-type stars from SIMBAD, we used the criterion query: $ra > 60$ & $ra < 75$ & $dec > 22$ & $dec < 31$ & $sptypes < A0$. This query (run in early 2011) resulted in 91 stars, three of which were listed twice with different names. We thus obtained 88 B stars and zero O stars through the SIMBAD database as candidates.

Second, potential Taurus members having early spectral types were taken from Tables 5 and 7 in Rebull et al. (2010). One of these, JH 225, also resulted from the SIMBAD search. Thus, the Rebull et al. (2010) paper added eight more stars with spectral types early A or B (O-type stars were absent). As noted above, the region covered by *Spitzer* does not encompass the whole region of our search (see Figure 2).

Third, we selected from the 2MASS-PSC [3] objects satisfying the same coordinates constraint used in the SIMBAD query, having $K_s < 10$ mag with $> 5\sigma$ detection, and no contamination or quality flags set. The brightness threshold places an upper limit on the visual extinction for the selected stars. For example, a B8V star can have a maximum visual extinction of $A_V \simeq 37$ to be selected, since the absolute K-band magnitude for such a star is $M_{K_s} = 0.11$, the distance modulus at 140 pc is 5.73, and the reddening law for 2MASS magnitudes is $A_K = 0.112 A_V$. Such a large value of extinction is much higher than the largest extinction observed for known Taurus members. The resulting 2MASS-PSC sample appears in the lower panels of Figure 3. These objects were further filtered through the photometric color criterion: $J - H < 1.698(H - K_s + 0.158)$ in order to select stars which, when translated backwards on the reddening vector in the $(J-H)/(H-K_s)$ color-color diagram, fall on the main-sequence earlier than spectral-type A0. For this procedure, we used intrinsic magnitudes from Kraus & Hillenbrand (2007), and the Rieke & Lebofsky (1985) reddening law, which is found consistent with reddening in the 2MASS photometric system (Maheswar et al. 2010). There is no a priori reason to believe that this color criterion will work well, due to one or more of the following reasons: (i) photometric errors could place stars within the reddening band employed in our selection; (ii) the reddening law (parametrized by R_V) is different for different lines of sight towards Taurus (e.g. Dobashi et al. 2005); (iii) stars of a given spectral type and luminosity class do not have unique photometric colors but tend to have a dispersion of astrophysical origin about the observed mean intrinsic value; (iv) additional emission of non-photospheric origin could change the $J - H$ and $H - K_s$ colors, possibly making late-type stars with infrared excesses look like earlier-type stars that are reddened; (v) stellar multiplicity is unaccounted for in our analysis. Nevertheless, using a more relaxed criterion is subject to the risk of selecting a large number of unreddened K and M-type stars which lie across the reddening vector defined by our photometric color criterion. Using our color criterion, we obtained 113 stars for further consideration. Fourteen of the stars selected in this manner were already present in the SIMBAD list of known early type stars (BD+23 607, HD 25487, V1137 Tau, HD 284228, HD 282240, HD 29259, 2MASS J04395574+2545020 = IC 2087, HD 283845, HD 283952, HD 31353, HD 284941, HD 284012, HD 283751, HD 283794) and so we added 99 early-type candidates through this criterion, which we appended to the working list. We also add the famous star AB Aur at this point, which would pass our color selection criteria but is formally excluded from our analysis based on 2MASS-PSC flags present at K_s-band.

Last, we added to our early-type candidates list the stars from the Finkbeiner et al. (2004) survey belonging to our spatial region of interest which are classified as spectral class O, B, or A based on low-resolution *SDSS* spectra. Finkbeiner et al. chose the program stars for spectroscopy as part of a survey seeking M-dwarfs, on the basis of red colors, or stars previously known as spectral class A or F for use as reddening standards. As noted above, the region covered by *SDSS* does not encompass the whole Taurus cloud (see Figure 2). Furthermore, there was no overlap between these candidates and those already selected above. We also considered a set of stars selected, similar to the 2MASS-PSC query described above, as those having $K_s < 10$ mag and blue colors within *SDSS*, specifically $u - g < 0$. This resulted in a short list of a few tens of objects, nearly all of which were known to SIMBAD already as early type stars (and thus included already among our first set of candidates), or as late type stars (with blue colors towards the blue, likely indicative of hot companions).

In addition to stars in the four samples considered above, HD 31305 (A0V) is a star which we found in the vicinity of Taurus-Auriga due to its early spectral type and proximity to the well-known Taurus member AB Aur, though it is not within the area of the Spitzer maps of Taurus.

Our final list of early-type candidates for membership in

[3] using the multi-object search form at the Infrared Science Archive (http://irsa.ipac.caltech.edu/)

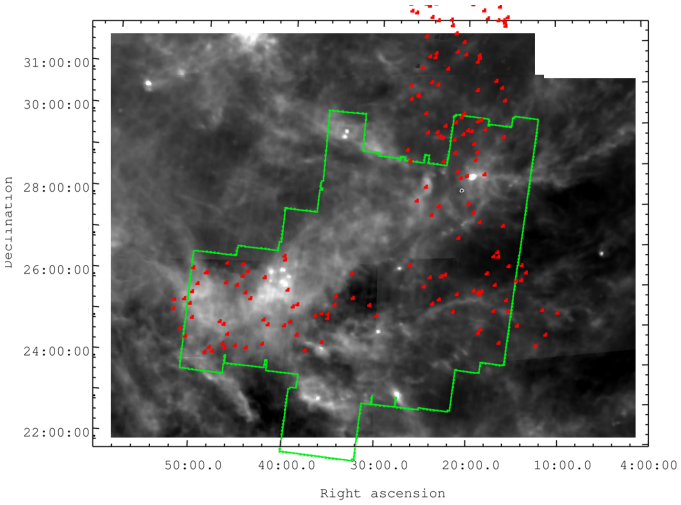

Figure 2. Areal extent of the Spitzer Taurus Legacy Survey (green) and SDSS spectroscopic observations by Knapp et al. (2007) (red symbols) overlaid on a mosaic of the Taurus region at 100μm from the *IRAS* Sky Survey Atlas.

the Taurus region of recent star formation thus consists of 329 stars. The color-color and color-magnitude diagrams for these stars, separated by the selection method, are shown in Figure 3. We then tested these objects for Taurus membership as described in the next subsection, after assembling the needed ancillary data.

For all objects in our list of candidate O, B, and A0 stars, we collected the following astrometric and photometric information. Proper motions were taken from the PPMXL catalog (Roeser et al. 2010), and trigonometric parallaxes from the Hipparcos catalog (Perryman & ESA 1997). B, V, and R magnitudes listed in the NOMAD-1 catalog (Zacharias et al. 2005), and J, H, K_s magnitudes from 2MASS-PSC were used. Radial velocity (RV, heliocentric) information was extracted from Gontcharov (2006) and Kharchenko et al. (2007) in that order of priority. For the *SDSS* stars which we chose from Finkbeiner et al. (2004), we used an A0 template to extract their radial velocities using the *SDSS* DR7 (Abazajian et al. 2009). In each of these catalogs, we searched for counterparts to our early-type candidate stars within 1 arcsec of the source position. In cases where two counterparts were found for a particular source, only the closest was considered. Finally, the spectral types were adopted from our own derivations for those stars which we followed-up spectroscopically (see section 2.4), from Rebull et al. (2010) for stars listed in that paper, from SIMBAD, or from the ASCC-2.5 catalog (Kharchenko & Roeser 2009), in that order of preference. We also performed a thorough literature search, seeking relevant data not available through large catalogs.

2.3. *SELECTION OF CANDIDATE MEMBERS OF TAURUS*

Physical association of astronomical objects can be established through the combination of common location and common space motion, with not all six dimensions available for every star. The case at hand is that of a star forming region lying at a mean distance of 140 pc and having a depth and transverse extent of $\gtrsim$ 20 pc. Although kinematics traditionally has been a robust mode of identification of cluster members, uncertainties in distance may lead to discrepant space velocities. Furthermore, the dispersion in the measured distance or kinematic quantities might be a significant fraction of their absolute values. With these challenges in mind, we chose the following filters to select (probable) members from our list of candidate early-type stars towards Taurus.

One set of criteria involved distance. Stars with trigonometric or spectroscopic parallax between 128 and 162 pc within 1σ errorbar were considered. Another set of criteria involved kinematics. From the probability associated with a calculated χ^2 statistic, stars having proper motion consistent with known members were selected. Finally, radial velocity (RV) was taken into account wherever available, considering as members stars with $9.8 \leq RV \leq 17.5$, which incorporates the mean radial velocities of all Taurus groups identified by Luhman et al. (2009) within 1σ uncertainty.

2.3.1. *DISTANCE CRITERION AND METHODS*

Through VLBI measurements, the distances to five Taurus members are accurately known (see Table 2 and for context Figure 4). Taurus is at least as deep as it is wide (Torres et al. 2009), a few tens of parsecs in each direction. Based on this, we assume that Taurus occupies the region between 128 to 162 pc (i.e. $6.2 < \pi < 7.8$ milli-arcseconds on parallax). From our list of early-type candidate stars we chose candidate Taurus members such that both their Hipparcos and spectroscopic parallax distances, within 1σ error, were consistent with the above-stated distance criterion. van Leeuwen (2007) has effectively demonstrated the validity of the Hipparcos parallaxes (however, see below for an argument against its validity for the case of HD 26212). We calculated the spectroscopic parallax distances for each of the six magnitudes (denoted by 'X' below) — B, V, R, J, H and K_s — using the definition,

$$d_X = 10^{(X - A_X - M_X)/5} \times 10 \qquad (1)$$

where $A_X = [B - V - (B - V)_0] \cdot R_V \cdot (A_X/A_V)$, $R_V = 3.1$, and $(A_X/A_V) = a + b/R_V$. The parameters 'a' and 'b' are from Table 3 of Cardelli et al. (1989), and are the best-fit parameters to the average extinction law. M_V is from Schmidt-Kaler (1982), intrinsic colors, viz. $(B-V)_0$, $(V-R)_0$ are from Johnson (1966), and $(V-K)_0$, $(J-K)_0$, $(H-K)_0$ colors are from Koornneef (1983). The Koornneef magnitudes/colors were transformed into the 2MASS JHK_s system using transformations from Carpenter (2001). This intrinsic color and magnitude information for O, B and A-type stars were compiled from Schmidt-Kaler (1982), Johnson (1966), Koornneef (1983) and Carroll & Ostlie (2006). BVR reddening was determined using Cardelli et al. (1989) with $R_V = 3.1$, and JHK_s reddening using Rieke & Lebofsky (1985). Stars with missing luminosity class information were assumed to be dwarfs. Candidates having spectral types for which the intrinsic magnitudes and colors are missing in our compiled tables necessitated interpolation between the two adjacent spectral types.

The error reported on the spectroscopic parallax distance is the standard deviation of the distances calculated using all

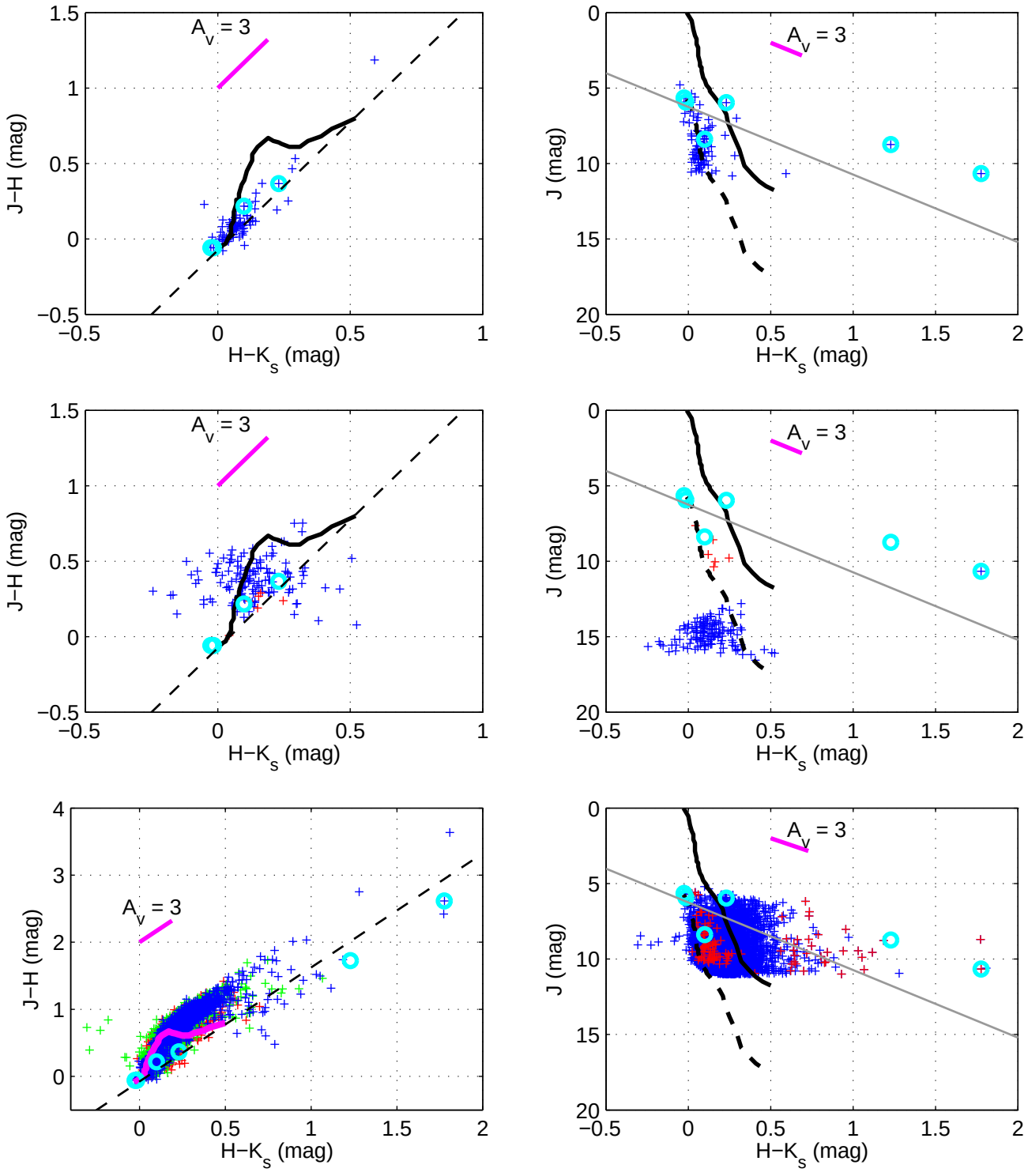

Figure 3. 2MASS color-color (left panels) and color-magnitude (right panels) diagrams for the early-type candidate stars considered in this work. 2MASS objects with contamination flags set and error in J,H,K_s magnitudes greater than 0.1 were rejected from the plots. The mean error in J,H,K_s magnitudes is about 0.02, which is smaller than the size of symbols used. *Top panels*: O,B stars from SIMBAD. In the color-color diagram, two of these stars lie outside the range plotted: V892 Tau (Elias 1) and IC 2087, having $(H-K_s, J-H) = (1.23, 1.73), (1.78, 2.62)$ respectively. *Middle panels*: Stars of spectral-type A and earlier from Knapp et al. (2007) are shown in blue. The B stars proposed by Rebull et al. (2010) are shown in red. Note that the area covered by these surveys is less than that represented in the top and bottom panels. *Bottom panels*: Left: 2MASS objects with color-coding as follows. Blue: stars with magnitude $K_s < 8$, green: $8 < K_s < 9$, red: $9 < K_s < 10$. Right: All 2MASS objects are in blue, and those selected as possible O,B stars using the photometric selection criterion (described in §2.2) are shown in red. *All panels*: The reddening vector (magenta) from Rieke & Lebofsky (1985) is used. Intrinsic colors and magnitudes of main-sequence stars (from Table 5 of Kraus & Hillenbrand 2007) are shown as a thick black curve (magenta curve in the bottom panel color-color diagram). The thick black, dashed curve in color-magnitude diagrams is the same curve, but displaced along the luminosity axis to denote the apparent magnitude of main sequence stars at 140 pc. The thin black, dashed straight line in the color-color diagrams represents the color-selection criterion applied to the 2MASS objects (see section 2.2). The thin grey solid line in color-magnitude diagrams represents the reddening vector passing through the position of an A0V star at a distance of 140 pc. The location of the six B stars illuminating bright IR nebulae are shown as cyan circles with two of the stars having very similar, near-zero, colors.

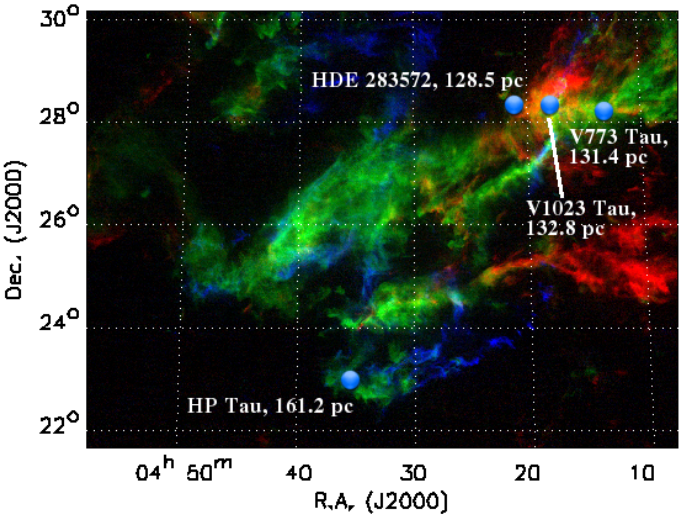

Figure 4. Distances to stars in Taurus measured via VLBI, from Table 2; the star T Tau is not shown since it lies south of the region of interest. Background image is velocity-coded ^{12}CO map from Goldsmith et al. (2008). The LSR velocities are color-coded as blue: 3–5 km s^{-1}, green: 5–7 km s^{-1}, red: 7–9 km s^{-1}.

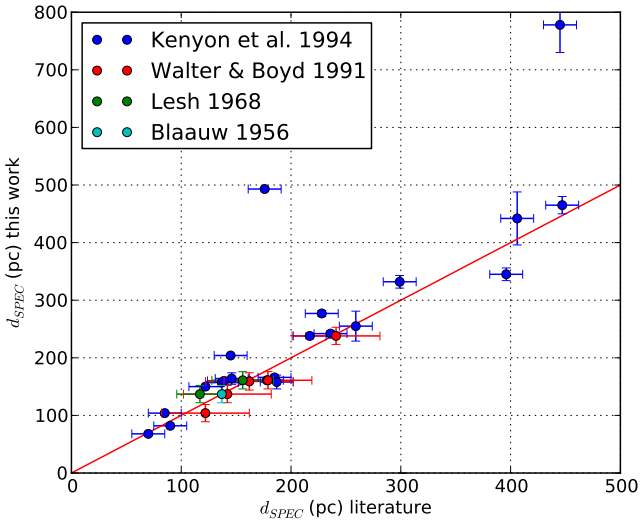

Figure 5. Comparison of spectroscopic distances calculated in this work with those published in past literature.

of the six magnitudes. Reliable estimates of intrinsic colors involving R,J,H and K$_s$ are not available for early-type giant stars, and hence we calculate the distance to the luminosity class III stars using only B,V magnitudes and color. Other errors that could contribute but have not been accounted for include: (i) spectral type / luminosity classification error, (ii) error in apparent magnitudes, (iii) intrinsic colors are mean values and do not account for astrophysical spread within the luminosity classes, (v) error in choice of reddening model, (vi) presence of non-photospheric emission such as infrared excess. For points (i) and (ii) stated above, the manner in which these criteria impact the distance estimate can be understood quantitatively via the discussion provided in section 3.3 of Kenyon et al. (1994). Following that discussion, the 1σ error on spectroscopic parallax corresponding to quantities (i) and (ii) is roughly 30 pc at a spectral type of A0 with $d = 140$ pc. This uncertainty would then add to our quoted error appropriately taking into account equation 1. Caution is thus advised in using the error bars quoted on spectroscopic distances, especially for giant stars.

Out of the 329 early-type candidates being tested for Taurus membership, the reddening and spectroscopic parallax distance can be calculated for 173 of them. In general, where there is overlap, the reddening values show good agreement with those stated in literature. We compare our averaged spectroscopic parallax distances with those determined by Kenyon et al. (1994), Walter & Boyd (1991), Lesh (1968), and Blaauw (1956) in Figure 5. For the majority of the objects, the spectroscopic parallax distances are in agreement within 1σ with those determined by *Hipparcos*. Notable exceptions are stars with very high reddening for which R_V (and possibly also the reddening law as a function of wavelength itself) would differ significantly from the value assumed here. Also, the method fails if the optical and/or near-infrared photometry is dominated by circumstellar rather than photospheric emission, or if the source is pre-main sequence rather than close to the main sequence; this latter condition is indeed the case for many of the later type stars selected in the 2MASS part of the search.

In considering the appropriateness of the distance criterion we have adopted for testing the association with Taurus, which is that all stars must lie between 128 and 162 pc, a problem arises in the unknown 3-dimensional shape of the molecular cloud. The cloud may extend further along some lines of sight, or it may not have high enough density for current star formation along other lines of sight. A related problem in establishing membership is that, to the west of Taurus, there is another star-forming region along the line of sight extending behind Taurus: the Perseus molecular cloud at about 350 pc. The spectroscopic parallaxes of HD 282276 and HD 283677 suggest that they both lie closer to the Perseus cloud, though on the sky they are aligned with Taurus, not the Perseus cloud; these stars also have similar proper motion (see below). There have been suggestions of a bridge of molecular material connecting the Taurus-Auriga and Perseus regions (Ungerechts & Thaddeus 1987) The presence of the somewhat older Cas-Tau OB association along the line of sight also poses a potential contamination problem because its members span a range of at least 30 pc in distance (de Zeeuw et al. 1999) and perhaps as much as 80 pc, although it is securely behind the Taurus star-forming region.

A method for distinguishing chance superpositions, in addition to the distance criterion, is to look at the kinematics of the stars and the natal cloud. Consideration of proper motion and radial velocity of the stars helps in eliminating ambiguity, as discussed in the next sub-section.

2.3.2. *KINEMATIC CRITERIA AND METHODS*

Kinematic membership probabilities are typically based on the convergent point method, which is used for regions that cover a large part of sky where the mean subgroup motion is changing as a function of position (this is a purely geometric effect). For regions less than a few degrees in size in the vicinity of comoving groups in Taurus, one can test the consistency of the proper motion of one star simply with respect

to the mean motion of a group. Luhman et al. (2009) computed the mean proper motions and radial velocities of eleven distinct groups (occupying 1–10 deg^2 on the sky; see Table 8 of that paper) of Taurus members. Seven of these groups, specifically I-V, VIII and X, lie within our region of interest.

We checked the statistical consistency between the proper motion of the candidate early-type stars reported in Table 3 and the proper motion of the closest kinematic group from Luhman et al. (2009) by estimating the χ^2 probability. The two components of proper motion, μ_α and μ_δ, can be understood as independent Gaussian variates drawn from a normal distribution parametrized by the mean (which can be estimated through the sample mean, i.e. the mean proper motion of the presently-known Taurus members) and the dispersion (likewise estimated as the dispersion of the sample of presently-known Taurus members). The sum of the square of these values will then be distributed according to the χ^2 distribution. Strictly speaking, these components are determined through the least-squares technique in proper-motion catalogs, and are correlated (the complete covariance matrix is, for example, provided by the Hipparcos catalog). Here, we have calculated the quantity χ^2 using the definition $\sum_{i=1}^{k}(x_i - \bar{x})/\sigma_i^2$, where $i = 1, 2$, and x_i describes the components of proper motion. The uncertainties, however, are associated with not only the proper motion of individual stars, but also with the sample mean. Further, we have to incorporate the internal dispersion of the presently-known members of Taurus. We calculated the χ^2 statistic and the associated probability using equations 2 and 3, after de Zeeuw et al. (1999):

$$\chi^2_{\nu=2} = \frac{(\mu_\alpha - \mu_{\alpha,\mathrm{group}})^2}{(\sigma^2_{\mu_\alpha} + \sigma^2_{\mathrm{int}} + \sigma^2_{\mu_{\alpha,\mathrm{group}}})} + \frac{(\mu_\delta - \mu_{\alpha,\mathrm{group}})^2}{(\sigma^2_{\mu_\delta} + \sigma^2_{\mathrm{int}} + \sigma^2_{\mu_{\delta,\mathrm{group}}})} \quad (2)$$

$$P(\chi|\nu) = \frac{\chi^{(\nu-2)/2} e^{-\chi/2}}{2^{\nu/2}\,\Gamma(\nu/2)} \quad (3)$$

where $\mu_\alpha, \mu_\delta, \sigma_{\mu_\alpha}, \sigma_{\mu_\delta}$ denote the proper motion in right ascension and declination of the star being tested and their associated uncertainties. The quantities $\mu_{\mathrm{group}}, \sigma_{\mu_{\mathrm{group}}}, \sigma_{int}$ are the proper motion of the Taurus group closest to the star, its uncertainty, and the intrinsic dispersion of proper motion in the group (assumed to be 2 mas yr^{-1}). The denominator of each term is then the expected variance of the respective numerators. This method traditionally has been used to find "proper-motion members", but is partly biased toward stars having a large relative uncertainty in their proper motion which reduces the χ^2. We are able to calculate the χ^2 probability for all of the 329 early-type candidate stars being tested for Taurus membership since their proper motion is known.

The result of this proper motion analysis is illustrated in the upper panel of Figure 6. The region allowed by our χ^2 probability membership criterion (set at $>1\%$) roughly corresponds to the shaded circular region. In the context of this figure, it is worthwhile to note that members of the background Cas-Tau OB association as listed by de Zeeuw et al. (1999) have μ_α ranging from a few mas yr^{-1} to 50 mas yr^{-1} (the mean is about 26 mas yr^{-1}), and μ_δ ranging from a negative few mas yr^{-1} to -40 mas yr^{-1} (mean is about -19 mas yr^{-1}; from the PPMXL catalog). Thus, a few of the stars studied herein are probably Cas-Tau members. A combined diagram showing the spectroscopic parallax distance and the proper motion of the early-type candidate stars is shown in the lower panel of Figure 6.

The RV dimension was not included in the χ^2 analysis because this quantity is unknown for most stars. In cases where it is known, the uncertainties are generally quite large. Thus, as the second component of our kinematics investigation, we compared the RV of each of the early-type candidate member stars (where available and as reported in Table 3) with that of the nearest Taurus group listed in Luhman et al. (2009). We chose as likely members the stars which, within 1σ, satisfied the criterion $9.8 \leq RV \leq 17.5$, corresponding to the range in the mean radial velocities of the Taurus groups. For the *SDSS*-selected early-type stars we show the radial velocities in Figure 7. Most of the *SDSS*-selected stars satisfying the nominal RV-selection criterion are too faint in the near-infrared to be probable members of Taurus.

2.3.3. *RESULTS OF CANDIDATE SELECTION*

The information in Table 3 was used along with the procedures outlined above to arrive at the list of likely early-type members of Taurus. In all, 52 stars independently satisfy the proper motion membership criteria and 28 the distance membership criteria, with 18 satisfying both. However, not all sources have known values for all or any of the quantities we consider. As the samples of early-type stars under consideration were derived from four different sources, we discuss the details of our analysis as appropriate for each sample in what follows.

For the SIMBAD sample of known early-type stars and for the Rebull et al. infrared excess sample, spectral types exist in the literature. Also, we have followed up some of these stars spectroscopically ourselves in order to verify or revise their spectral classification. Fairly accurate spectroscopic parallax distances have thus been used to test the membership of these two sets of stars with Taurus. Radial velocity measurements also exist for some of these stars. We found that two stars, HD 28929 (B8V; also known as HR 1445) and HD 29763 (B3V; also known as τ Tau), satisfy all the tested criteria for membership of Taurus: parallax distance, proper motion, and radial velocity. V892 Tau (A0; also known as Elias 1) satisfies the first two criteria, leaving the third unknown due to insufficient information, but this star is already an accepted member of Taurus on the basis of its circumstellar disk attributes.

In the 2MASS photometric sample, accurate spectral classification is absent for many of the stars, and hence for these, the calculation of accurate spectroscopic parallax has not been possible. In this set of stars, twelve satisfy two criteria leaving the third criterion indeterminate due to insufficient information, while two stars satisfies all the criteria for membership of Taurus. However, many of these stars are late type T Tauri stars that are already known members of Taurus but selected

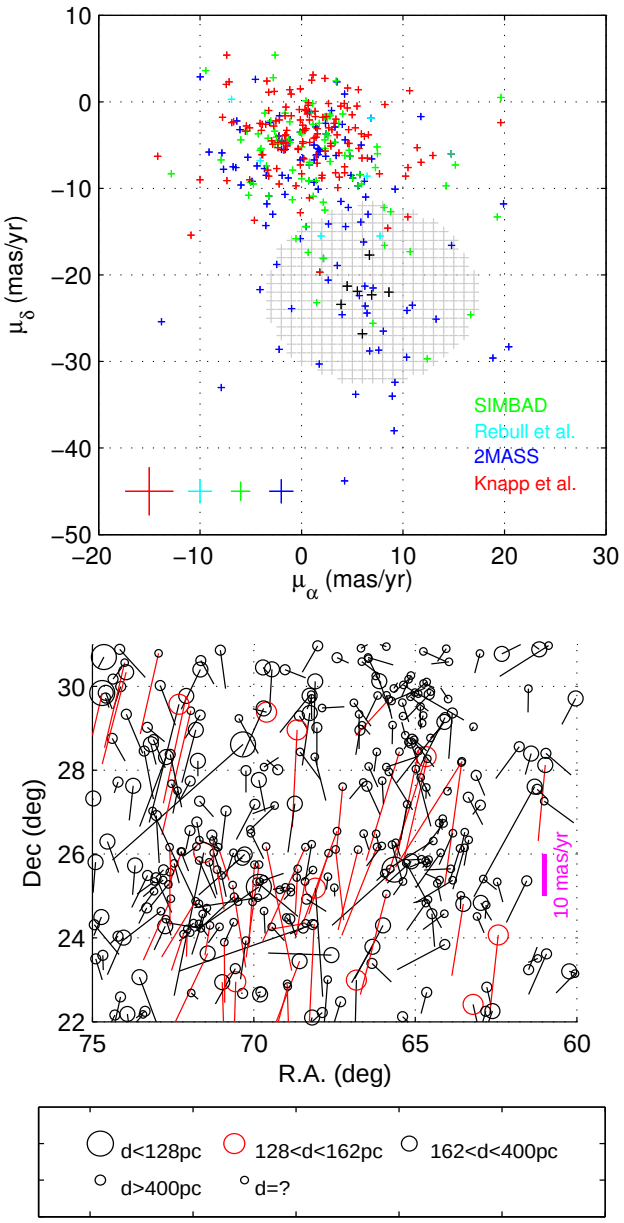

Figure 6. *Upper panel*: Proper motions of the candidate early-type stars shown as a cloud plot with blue indicating objects selected from 2MASS; green, SIMBAD; cyan, the B stars proposed by Rebull et al. (2010), and red: O,B,A stars from Knapp et al. (2007). The "+" symbols at the bottom-left corner denote the mean errors for each sample. The mean proper motion of Taurus groups considered in this paper (see Section 2.3.2) are shown as black symbols The hatched reference circle indicates the area where the χ^2 probability of membership is greater than 1% with respect to the mean proper motion of Taurus. 51 stars from our list of candidate early-type stars have proper motions consistent with Taurus groups. *Lower panel*: Vector diagram showing the proper motion of all the stars tested for membership. Those which satisfy the proper motion criterion P($\chi^2 > 1\%$) are shown in red. Positions of the stars are indicated by the circles, whose sizes are based on the spectroscopic parallax distance of the respective stars (key given at the bottom). Red circles denote stars satisfying our distance criterion for Taurus member selection (within an uncertainty of 15 pc).

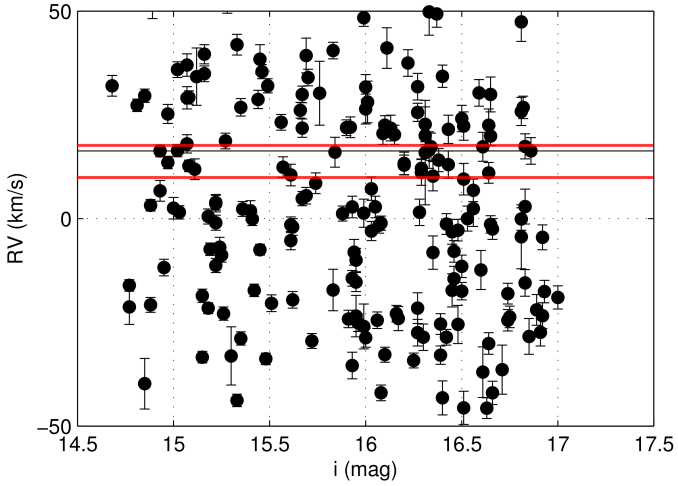

Figure 7. A plot of radial velocity against *SDSS* i-band magnitude for the early-type stars selected from Knapp et al. (2007). The y-axis has been rescaled to show only the stars with RV between $\pm$50 km s^{-1}. The mean RV of accepted members of Taurus (Luhman et al. 2009), 15.8 km s^{-1}, is shown with a black horizontal line. The neighboring red lines denote the region $9.8 \leq RV \leq 17.5$, our RV-member selection criterion. Among those stars which satisfy this RV criterion, most are too faint to be probable members of Taurus.

by our methods because they have large enough near-infrared excesses to push them into the region of the 2MASS color-color diagram occupied by reddened earlier type stars. We note that the 2MASS search does select the mid-A stars HD 26212 and HD 31648 (along with AB Aur, if we ignore the 2MASS-PSC flag at K_s-band) as candidate early-type members, but finds no new B stars.

For the *SDSS* spectroscopic sample, the magnitude range precludes the availability of any *Hipparcos* parallax values, but since spectral types are available for many stars, spectroscopic parallaxes can be calculated. RV is also measured by the *SDSS* analysis pipeline. Some of the *SDSS*-selected stars satisfy the kinematic criteria (see Figures 6 and 7); however, they are under-luminous with respect to the expectations for reddened early type stars at the Taurus distance (see middle panels of Figure 3) and indeed have much larger spectroscopic distance estimates (Table 3). Most of these early-type stars are likely in the Galactic halo.

Finally, the spectroscopic parallax distance suggests that HD 31305 (located near AB Aur and discussed by Cody et al. (2013)) lies just beyond the distance range defined by our member-selection criterion ($<$10% in excess of the standard deviation among calculated d_{SPEC} values). Nevertheless, its proper motion conforms with that of known Taurus members. Hence, we consider in what follows that this star could well be a member of Taurus.

In summary, we newly advocate the membership of two B-type stars (HD 28929 and HD 29763) and one A-type star (HD 26212) in Taurus using distance and kinematic arguments, and in addition find one A0-type star (HD 31305) to be a probable member (though it is not yet confirmed due to the lack of radial velocity information). Below, in section 3, we discuss these stars in more detail and also revisit some of

those which were rejected in the above procedures. After consideration of other evidence which might point towards their association with Taurus, we find several additional B and A0-type to be plausible Taurus members. In order to inform our further assessments regarding the likelihood of cluster membership, additional data on many of these stars was collected.

2.4. *FOLLOW-UP SPECTROSCOPY*

We performed follow-up spectroscopy of selected stars with an aim of (i) confirming or revising their spectral types based on temperature and surface gravity diagnostics, (ii) measuring radial velocities, and (iii) determining more precise stellar parameters so as to estimate ages. We obtained optical spectra for a subset of the Taurus early-type candidates which were found to satisfy several of our membership criteria, or which illuminated a nebula in the Spitzer image. Some of these sources appeared to be better candidates at the time we obtained the spectra than later re-analysis revealed. We also observed for comparison a grid of dwarf B stars from Abt et al. (2002). and, for calibration, RV standard stars and spectrophotometric standards.

The optical spectra were obtained at the Palomar 200-inch Hale telescope on 4 December 2010 using the Double Spectrograph (DBSP). The data have medium spectral resolution ($R \simeq 7800$ and 10419 in the blue and red channels respectively). We used a dichroic at 5500Å to split the optical light into blue and red channels with a 1200 lines mm^{-1} grating blazed at 4700Å, at a grating angle $34.92°$ on the blue side and 1200 lines mm^{-1}, 7100Å blaze, and $42.73°$ on the red side. The spectral range covered was $\sim 3480 - 5020$ Å at 0.55 Å pixel^{-1} (blue) and $\sim 6440 - 7110$ Å at 1.4 Å pixel^{-1} (red). For wavelength calibration we used an Fe-Ar lamp in the blue and a He-Ne-Ar lamp in the red. Spectra for two stars (HD 27659 and HD 26212) were taken on 2 September 2011 using a different configuration resulting in a much lower resolution and a larger wavelength coverage.

We reduced the data using the Image Reduction and Analysis Facility (IRAF) *ccdred* and *onedspec* packages. Spectra were extracted with the *apall* task after trimming, bias-subtraction, and flat-fielding of the images. The wavelength solution was then applied using *dispcor*. In the case of stars for which we had multiple short-exposure observations, the spectra were coadded using *scombine* to get a higher signal-to-noise ratio. We normalized all the spectra with *splot*.

For spectral typing the program stars, we measured the equivalent widths of several diagnostic absorption lines using *splot*, and then compared them with those of reference-grid stars (Figure 8), guided by the graphics in Didelon (1982). The normalized spectra of the reference-grid stars and the program stars are shown in Figure 9 with the reference types adopted from the literature and the program star types derived by us. We also compared our spectra with templates by Gray[4] and Morgan et al. (1943)[5]. The results of the spectroscopic analysis are given in Table 4. Estimates for the effective temperature ($T_{\rm eff}$), projected rotational velocity ($v\cdot \sin i$) and the surface gravity (log g) and were made by fitting the spectra with templates from Munari et al. (2005). For the template spectra, the comparison grid resolution was 500–1000 K in $T_{\rm eff}$ and 0.5 in log g, while the grid in $v\cdot \sin i$ was: 0, 10, 20, 30, 40, 50, 75, 100, 150, 200, 250, and 300 km s^{-1}; hence, our derived values are no more accurate than this. Some stars have equally good fits between a higher temperature and gravity point, versus a lower temperature and gravity point one grid spacing away; in these cases we generally preferred the dwarf to the giant solution. The physical parameters derived from this fitting are given in Table 5. In combination with the set of intrinsic stellar parameters discussed above, we thus derived a second set of spectral types for the stars that were spectroscopically followed up. These spectral types generally agree with those derived using equivalent widths in Table 4. Due to the coarse spectral grid of templates and degeneracies involved in the fitting process, the spectral types derived from our equivalent width analysis usually take precedence over those derived from spectral fitting.

Unfortunately, radial velocity information could not be derived from our spectra at the expected performance of the instrument (given our care in taking source-by-source comparison lamp calibration frames), perhaps due to poorly understood flexure effects. We note that an error as small as 1 Å in the wavelength calibration leads to an error of about 66 km s^{-1} at 4500 Å. Shifts of this order have been experienced between contiguous exposures while working with DBSP data. Due to our short exposure times, there are no sky lines in the blue part of the spectrum that could aid in more accurate wavelength calibration. While the red channel spectra have ample telluric absorption, too few photospheric absorption lines are available to provide a good fit. Hence, we defer the estimation of RV to a later time with another data set.

Notably, hydrogen emission lines or line cores are seen in HD 283751, HD 283637, V892 Tau, and AB Aur (see Figure 9). While the emission properties of the last two stars in this list are well known, they are not widely appreciated in the first two objects. Emission lines are often taken as a signature of activity associated with stellar youth, although evolved early-B type stars may exhibit a "Be phenomenon". We note that the derived spectral types of these emission-line objects are B5e and B9.5e, later than typical of evolved Be stars, but the infrared excesses detected by Rebull et al. (2010) are more typical of evolved Be stars than of young accretion disk systems. Neither star can be associated with Taurus by kinematic or distance arguments, and thus they appear to be interesting background interlopers.

A further note concerning the spectra is the appearance in Figure 9 of what is likely diffuse interstellar band absorption at 6614 Å in about half of the program stars. Corresponding broad absorption at 4428 Å is also seen. There is excellent correlation between the presence of this feature and the spectroscopic parallax distance estimates reported in Table 3. Distant stars have the absorption while closer stars do not. Notably, none of the stars we eventually conclude in this work to be associated with Taurus have these interstellar absorption features.

Finally, we note that the absorption at 6708 Å, coincident

[4] http://ned.ipac.caltech.edu/level5/Gray/Gray_contents.html
[5] http://ned.ipac.caltech.edu/level5/ASS_Atlas/MK_contents.html

with the Li I line seen in young low mass stars, is not likely to be astrophysical given its ubiquitous appearance in our spectra taken on 2010, December 4 (Figure 9); we suspect a (currently unexplained) terrestrial origin.

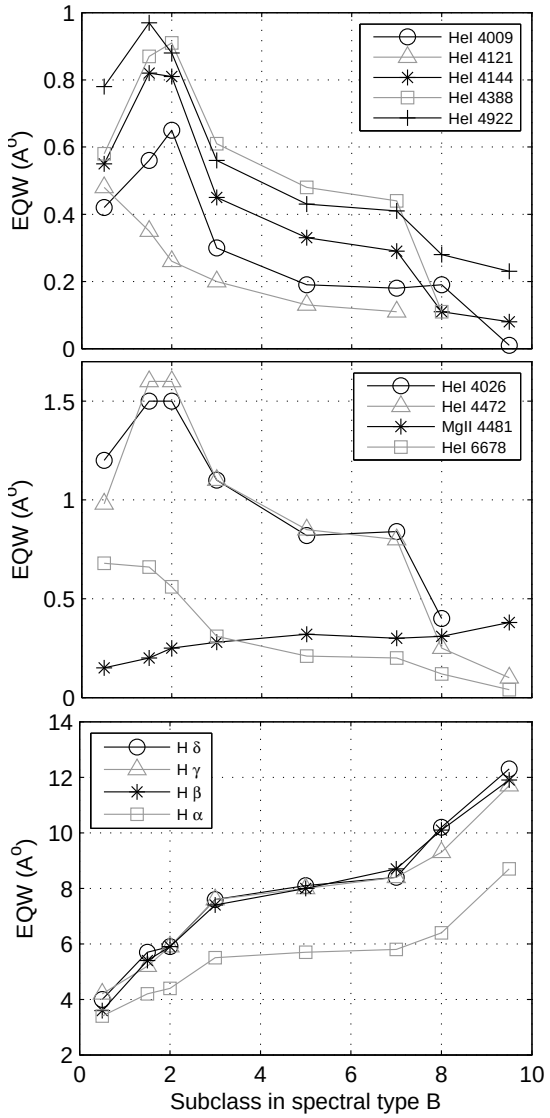

Figure 8. Equivalent widths of various absorption lines measured in the grid of B-type spectral standard stars (luminosity class V only) that were observed for comparison with the Taurus candidate early-type stars.

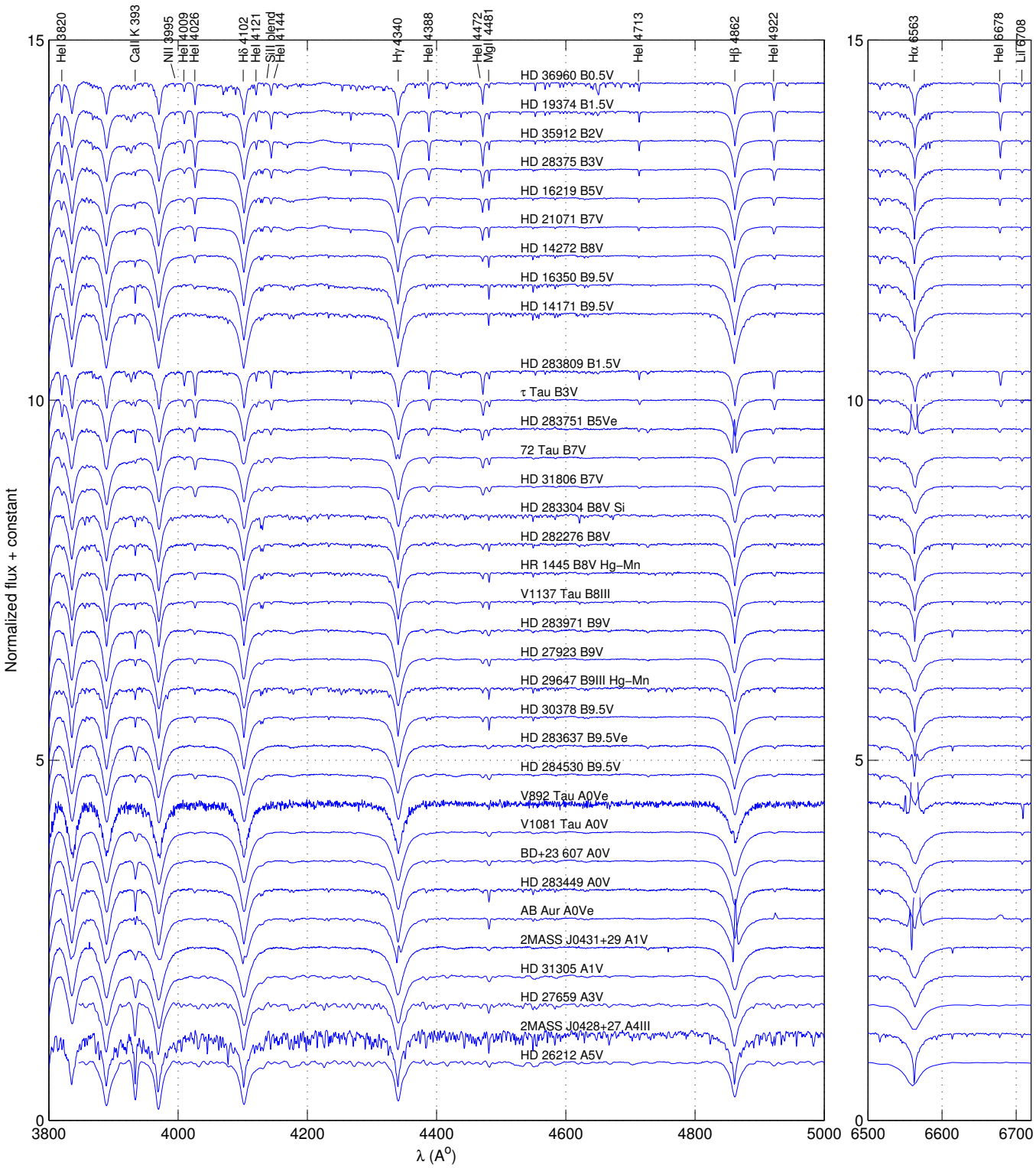

Figure 9. Normalized optical spectra obtained at the Palomar 200-inch Hale telescope. The upper set of stars comprise the grid of B-type spectral standard stars used for assigning spectral types to the program stars (lower set of spectra). All spectra have an arbitrary offset along the ordinate. Note the hydrogen emission lines or line cores in HD 283751, HD 283637, V892 Tau, and AB Aur. Approximately half of the program stars have diffuse interstellar band signatures: a narrow absorption at 6614 Å and a broader shallow feature at 4428 Å. The feature labeled as Li I 6708Å in the right panel is probably anomalous as this line is not expected to be present in these early-type young stars, and especially not in the spectral standards (including our white dwarf flux standard which is not shown); we suspect a possible terrestrial atmosphere source, perhaps associated with the Geminid meteor shower; this hypothesis is supported by lack of absorption at this wavelength in the two spectra towards the bottom of the sequence that were taken on a different night from all others.

3. INDIVIDUAL EARLY TYPE OBJECTS PLAUSIBLY ASSOCIATED WITH TAURUS

In this section we consider the collective set of plausible early-type members of Taurus based on the various lines of evidence for their physical association with the clouds.

Above we discussed the kinematic and distance evidence for association of HD 28929 (HR 1445), HD 29763 (τ Tau), HD 26212, and HD 31305 with Taurus. Additionally, the early type sources HD 31648, AB Aur, HD 27659, and HD 283815 have several lines of evidence that favor their association with Taurus but do not meet all of our stated criteria, mostly due to missing data.

Further, within the footprint observed by Spitzer, six B-type stars (IC 2087, 72 Tau, V892 Tau, HD 282276, HD 29647 and HR 1445) are seen in multiband images to illuminate mid-infrared reflection/scattered-light nebulae, not all of which can be kinematically associated with Taurus. As mentioned above, HR 1445 was also picked out by our distance and kinematic membership selection criteria. Indeed, the discovery of the bright nebulae in the Spitzer images was our initial motivation for this investigation. The nebular structure is illustrated in Figures 10 – 15. With the exception of IC 2087 which has a bright optical nebula, optical scattered light is weak or absent among our sample. Furthermore, there is relatively little extended emission in the near-infrared (J, H, K_s bands), with the wavelength of peak emission in the nebular regions typically being 8 or 24 μm. The morphologies of the nebulae are quite varied. They extend up to a few arcminutes and can appear circular or squarish, some of them being asymmetric and highly striated.

For both kinematically selected and nebular-selected objects, we constructed spectral energy distributions (SEDs) as shown in Figure 16. We used the following data in making the SEDs: (i) sub-mm: SCUBA/Andrews & Williams (2005); (ii) infrared: *Spitzer*, 2MASS, AKARI, IRAS; (iii) optical/UV: NOMAD, GALEX. Counterparts within one arcsecond of the source were chosen, with the exception of IRAS counterparts.

For young pre-main sequence stars, red *Spitzer*/IRAC colors indicate excess emission from circumstellar disks and envelopes, whereas excess emission at 24 μm but not in the shorter wavelength IRAC bands is indicative of a disk with an inner hole. At slightly later stages the dust is attributed to second generation 'debris' rather than primordial material. Infrared excess also could be attributed to dust shells around evolved stars, or illumination of nearby interstellar material, irrespective of any physical association of it with the star.

We also constructed various color-magnitude diagrams and overplotted isochrones (see Figure 17) to assist in the assessment of stellar age, assuming that the distance of Taurus is appropriate for each source. The unknown stellar multiplicity and photometric error add substantial uncertainty to the stellar age estimate. Also, because of the rapid evolution of high mass stars, the age derived via isochrones is very sensitive to the reddening correction, which is not insignificant, and which we have derived assuming a plausibly invalid constant R_V of 3.1. All these factors together preclude accurate determination of the stellar ages of our sample but we present the resulting color-magnitude diagram for completeness.

We now discuss our findings for individual sources, beginning with those illuminating nebulae in the *Spitzer* and then moving on to other candidates that we have assessed.

3.1. *IC 2087*

The IC 2087 nebula (Figure 10) is brightest at optical wavelengths and is less prominent at *Spitzer* wavelengths, a unique illumination pattern among our sample. The SED (Figure 16) of the associated point source (IC 2087-IR or IRAS 04369+2539 or Kim 1-41) is consistent with an early-type Class I – Class II young stellar object seen through $\sim$15 magnitudes of visual extinction. The foreground extinction is claimed to be $A_V < 1$ (Frerking et al. 1982), and hence the majority of the extinction toward IC 2087 should be due to circumstellar material (Shuping et al. 2001).

This source is a known YSO member of Taurus. High veiling has precluded accurate determination of its spectral type but Elias (1978) classified it as B5 based on the bolometric luminosity. We were unable to derive a spectral type from either the *SDSS* spectrum or our own follow-up optical spectroscopy of this source. No spectroscopic parallax is possible given the vague spectral type. However it appears that a proper motion measurement exists for IC 2087. White & Hillenbrand (2004) quoted a radial velocity of 22 ± 8 km s^{-1} but with the large error bar it is hard to tell whether the measurement is consistent with the RV membership criterion used herein; furthermore, the lines used may have been dominated by outflow kinematics rather than photosphere. Nonetheless, the source is currently an accepted member of Taurus, and based on multiwavelength information, we propose that an early spectral type of B5–B8 is most appropriate.

Rebull et al. (2010) confirmed that the source has a flat spectrum in the near-to-far-infrared, and report $L_{IR}/L_{total} = 0.41$. Weak molecular outflows, the presence of Herbig-Haro knots, mid-IR absorption features and associated reflection nebulosity provide additional evidence of the pre-main sequence nature of this object (e.g. Furlan et al. 2008). Hillenbrand et al. (2012) provide an extensive discussion of this source.

3.2. *72 Tau*

The nebula associated with 72 Tau (HD 28149) is brightest at about $\sim$ 60 μm. It is prominent in all IRAS and *Spitzer* bands and is also discernible in the optical bands. From the image cutouts (Figure 11) it is evident that the optical depth of the associated nebula is quite different at different wavelengths in the infrared. The nebular morphology is similar to that observed for the Maia nebula, illuminated by the Pleiades stars. The SED (Figure 16) of 72 Tau source is consistent shortward of about 10 μm with an ideal blackbody having very low reddening, but there is a longer wavelength excess. The SED morphology is similar to that of Maia as well. Kalas et al. (2002) noted that 72 Tau is a Vega-like source associated with a gas overdensity, but no rigorous analysis was performed. In section 4, we present a *DUSTY* model for the SED.

We arrive at a spectral classification of B7V for 72 Tau

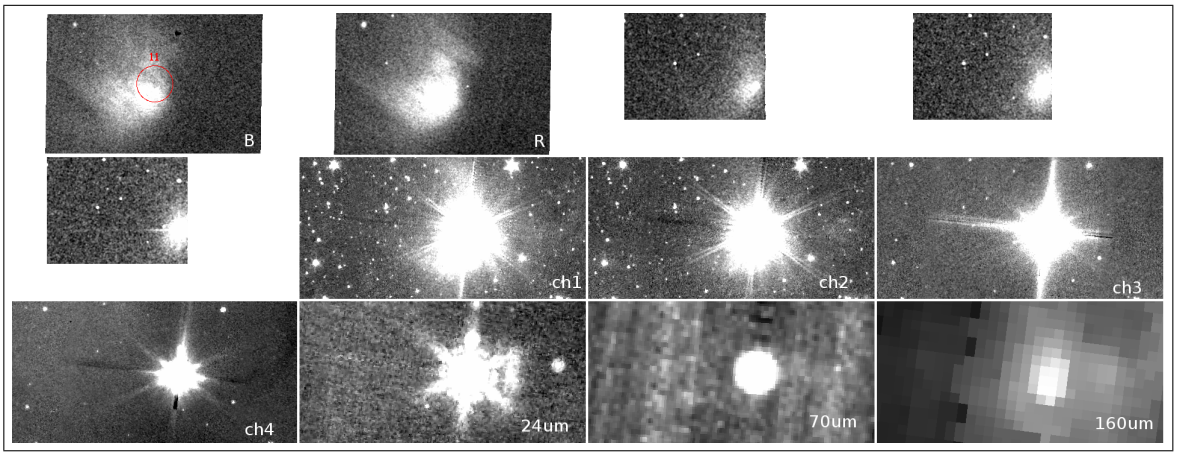

Figure 10. Cutouts of the IC 2087 region. Left-to-right are: B, R images from the Palomar Observatory Sky Survey (POSS-I) and J, H images from 2MASS (Row 1), Ks band from 2MASS, and IRAC channels 3.6μm, 4.5μm, 5.8μm (Row 2), IRAC 8μm, and MIPS images 24μm, 70μm, and 160μm (Row 3). The red circle in the POSS-I B band image has a diameter of 1 arcmin, for scale.

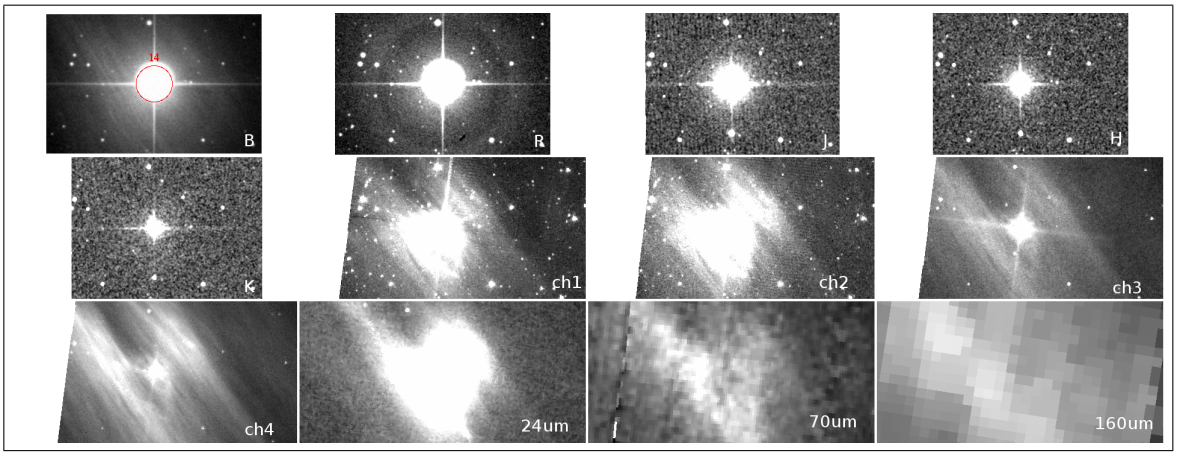

Figure 11. Same as Figure 10 but for 72 Tau.

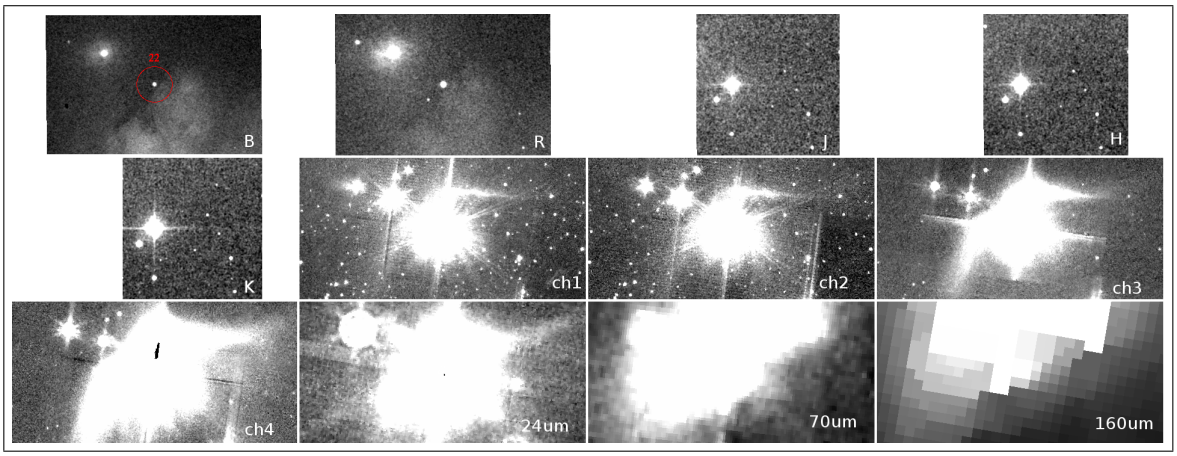

Figure 12. Same as Figure 10 but for V892 Tau / Elias 1.

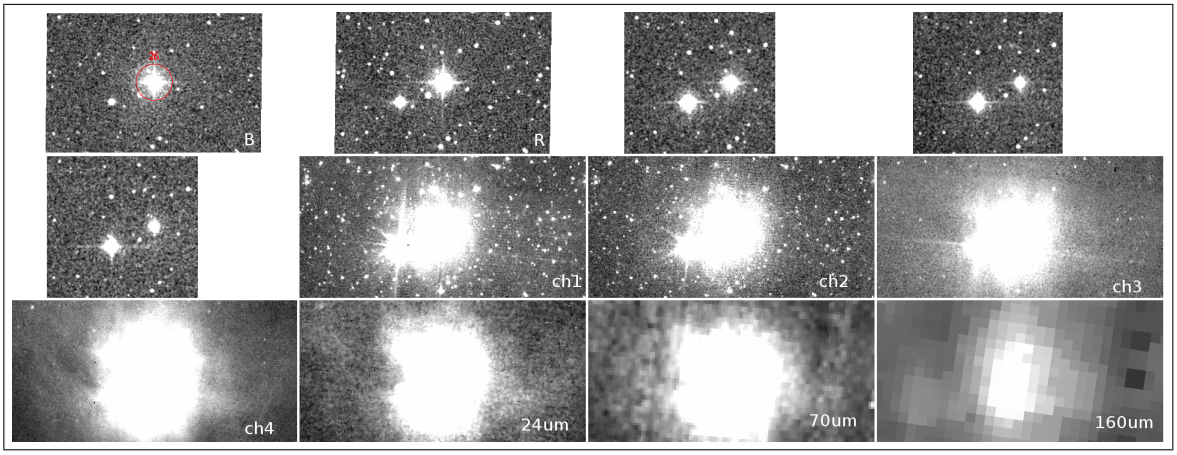

Figure 13. Same as Figure 10 but for HD 282276.

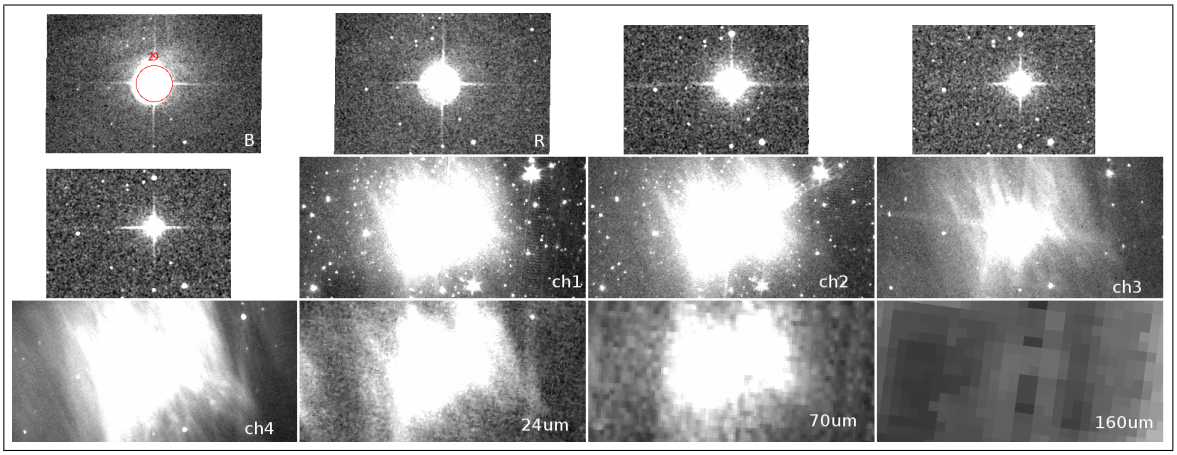

Figure 14. Same as Figure 10 but for HD 29647.

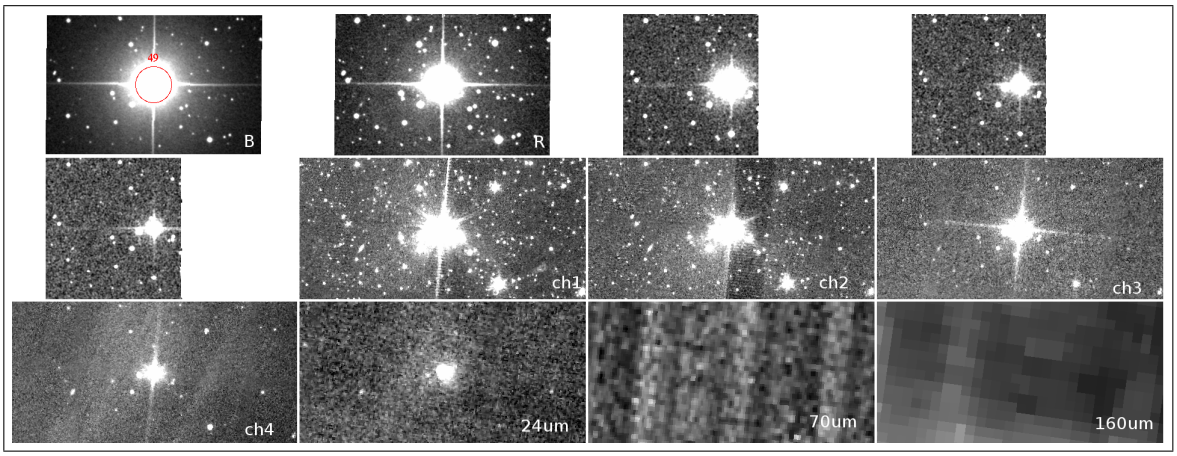

Figure 15. Same as Figure 10 but for HR 1445.

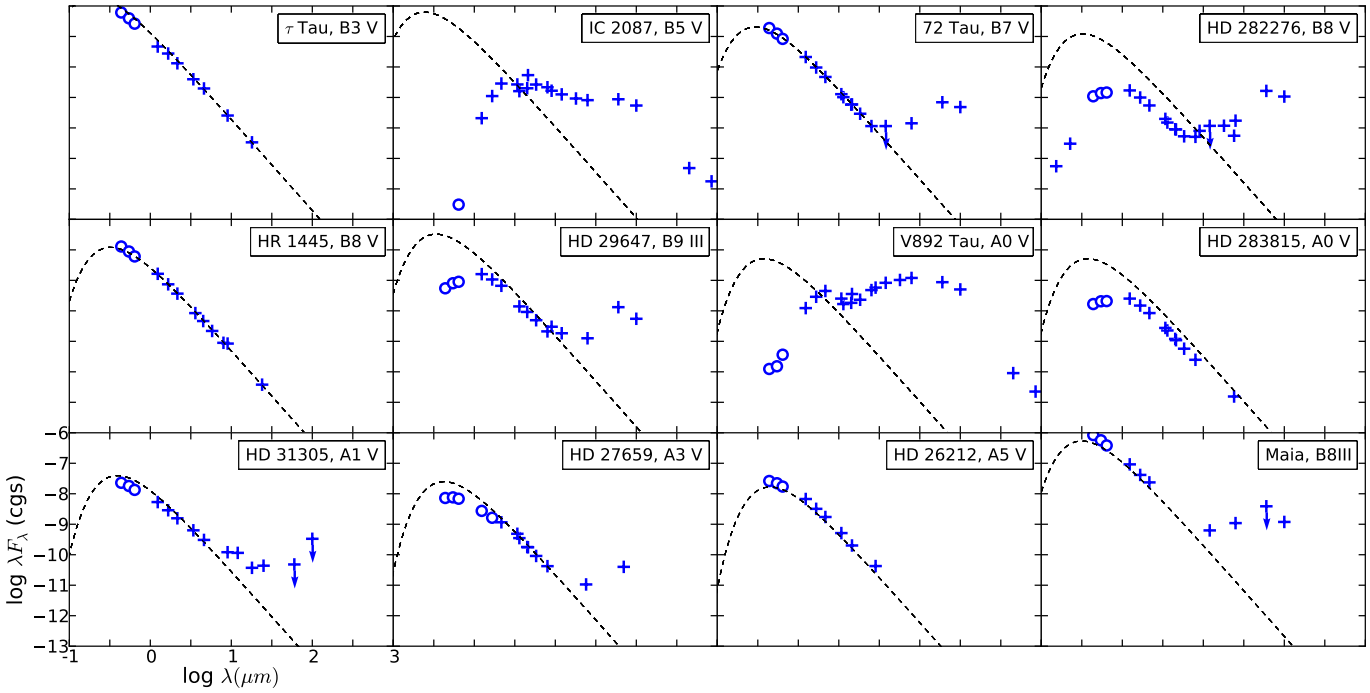

Figure 16. Spectral energy distributions (SEDs) of those sources exhibiting infrared nebulae in Figure 1 plus the candidate early-type stars we conclude are probable members of Taurus based on our assessment of distance and kinematics. Infrared excess is apparent in many objects. This may be due to the presence of a circumstellar disk associated with a pre-main sequence stars, to a debris disk in a somewhat older main sequence star, to a dusty atmosphere in the case of an evolved giant star, or to a chance superposition of a hot star with a nearby diffuse cloud. For comparison, an example of the chance-superposition case is also shown in the lower right panel: the Pleiades member Maia, whose SED exhibits an apparent infrared excess. The data sources include GALEX (ultraviolet), NOMAD (optical, BVR), 2MASS-PSC (near-infrared, JHK_s), *Spitzer*, AKARI and IRAS (mid-far infrared), and SCUBA (sub-mm). Photometric error bars are generally smaller than the symbol size; circles denote photometry lacking uncertainty (usually values from NOMAD). The dashed line in each panel represents a blackbody at 140 pc characterized by the effective temperature and radius of the star whose SED is represented in that panel. No correction for reddening has been applied though the existence of reddening can be inferred from the location of short wavelength photometry well below the nominal blackbody.

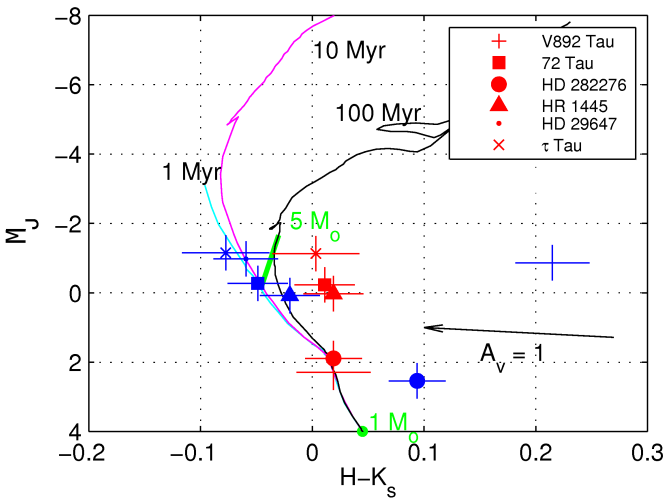

Figure 17. Estimation of the isochronal age of some of B stars showing infrared reflection nebulae and τ Tau. Isochrones are from Girardi et al. (2002). Horizontal errorbars represent the error in the 2MASS magnitudes and vertical errorbars represent the uncertainty in the distance ($128 < d < 162$pc). Blue markers are plotted using the reddening parameters from literature, while red markers represent values derived using $R_V = 3.1$ and the Cardelli et al. (1989) reddening.

based on our follow-up spectroscopy. The Hipparcos distance to this star is 127 ± 12 pc while our estimate of spectroscopic parallax is 161 ± 3 pc. Walter & Boyd (1991) quoted a spectroscopic parallax distance of 179 pc and proposed that this star is a member of Taurus and the Cas-Tau OB association. The study by de Zeeuw et al. (1999) however does not acknowledge this star as a member of Cas-Tau association. If the Hipparcos distance is accurate, then 72 Tau would lie close to the nearer edge of the Taurus cloud. Both the proper motion and the radial velocity of this star are consistent with the Taurus group (as defined by Luhman et al. 2009). We conclude that it is very likely that 72 Tau belongs to Taurus, although in the past the star has been considered a background source in studies of the TMC cloud.

Caution is suggested by the Pleiades-like striated nebulosity. It should be noted that the radial velocity of Pleiades members does not closely match that for the foreground nebula, unlike the case of 72 Tau. Previous age analysis in the literature (Westin 1985) suggested an age of 20 Myr based on ubvyβ photometry and theoretical stellar evolution models. From our spectral analysis, 72 Tau is clearly a main-sequence star which, after consideration of its spectral type, tells us that it is at least several Myr old and at most 170 Myr old; we are unable to place any further constraints on its age.

3.3. *V892 Tau*

In the optical bands, V892 Tau (also known as Elias 1 or more properly Elias 3-1) appears to be a point source with an associated faint reflection nebula (Figure 12). The nebular structure is brightest at about 24μm. Like IC 2087-IR, it is heavily reddened with a significant envelope component to its circumstellar environment. The SED (Figure 16) is that of a Class I – Class II source. Rebull et al. (2010) report it as a flat-spectrum source in the near-to-far-infrared, having $L_{IR}/L_{total} = 0.089$. V892 Tau is a double-star system (Smith et al. 2005) with a circumbinary disk (Monnier et al. 2008).

This Herbig Ae/Be system is a well-accepted member of Taurus with reported spectral types ranging from B8 to A6. Our spectral type is B8.5V to ∼A0Ve. The optical spectrum also shows Balmer emission lines, further evidence of its youth and likely membership. Our derivation of the spectroscopic parallax distance for this star has a large uncertainty, possibly enhanced by reddening law uncertainties. The probability associated with the χ^2 analysis confirms that this source is a proper-motion member of Taurus.

3.4. *HD 282276*

The nebula associated with HD 282276 (Figure 13) is evident only in the *Spitzer*/IRAC and MIPS bands, and not in the 2MASS or shorter wavelength bands. The nebula appears to be circular and optically thick at *Spitzer* wavelengths. This source shows considerable infrared excess in its SED (Figure 16) beyond 10 μm. The two peaks in the infrared excess suggest two different dust components from either two different radii or two different compositions contributing to the infrared emission. In section 4 we present a *DUSTY* model for the SED.

Rebull et al. (2010) have classified HD 282276 as a pending member of Taurus which needs additional follow-up; they tentatively categorized it as a Class II YSO. The spectrum of this star is B8V in our analysis but it does not show any emission lines. Both the spectroscopic parallax distance and the proper-motion are inconsistent with Taurus. We estimated the reddening to be $A_V = 2.8$, and a spectroscopic parallax distance of 422 ± 52 pc, which means that it lies closer to the distance of Perseus than Taurus. We speculate that this star could be associated with the Perseus star forming region, which has a mean proper motion of about $\mu_\alpha = 5$ mas yr^{-1}, $\mu_\delta = -12$ mas yr^{-1} (de Zeeuw et al. (1999) and PPMXL catalog), quite consistent with the measured values for HD 282276. However, the derived distance is somewhat large, even for Perseus and the star is offset to the east of the main Perseus cloud. There is no radial velocity measurement. Indeed, HD 282276 historically has been used in studies of the molecular cloud's physical and chemical properties under the assumption that it is a background source.

The fact that the star illuminates a reflection nebula in the infrared (see Figure 1), suggests the presence of cloud material, perhaps associated with a low column density extension of the classical Perseus region. It is also possible that the case of HD 282276 is similar to that of several Pleiades member stars, with the star randomly encountering a local overdensity in the interstellar medium.

3.5. *HD 29647*

Multi-wavelength images of HD 29647 (Figure 14) clearly show striated nebulosity similar to that associated with Pleiades stars. Even the SED is similar to that of Maia, a Pleiades member; both are shown in Figure 16. In section 4 we present a *DUSTY* model for the SED of this source.

HD 29647 is described in the literature as a heavily reddened Hg-Mn B6-7 IV or B8III star. From our spectrum, we classify it as a B9III spectral type and can confirm the presence of Hg absorption. Our analysis shows a spectroscopic parallax distance of 160 ± 1 pc, consistent with Taurus membership. However, as we do not have reliable estimates for the intrinsic colors of B-type giant stars, this distance estimate might have systematic error much greater than the quoted uncertainty. Whittet et al. (2004) argue that the visual extinction of 3.6 magnitudes for HD 29647 and 5.3 magnitudes toward an adjacent sightline suggests that this star lies within a cloud that is slightly beyond TMC-1, but within the diffuse screen surrounding a dense cloud clump. The Hipparcos parallax distance to HD 29647 is 177 ± 35 pc, suggesting that it is probably close to the farther edge of the molecular cloud. Based on proper motion analysis, the star is probably a non-member; there is no radial velocity estimate.

The fact that HD 29647 illuminates a bright infrared nebula is, however, a compelling reason to associate this star with the far side of Taurus as Whittet et al. have suggested. A scenario where HD 29647 was born from the Taurus cloud and ended up having different motion can be envisaged (for example, through ejection from a binary/multiple-star system). Given the relatively low space velocity as estimated from the small proper motion, however, this scenario seems unlikely. Perhaps it was born from a cloud lying between the present-day Taurus and Perseus clouds. Being a giant star, an age between 90 Myr and 120 Myr as deduced from stellar evolution models, may be appropriate for this ∼5 $M_\odot$ star. We conclude that the nebulosity in this case is a similar situation to that of Pleiades stars.

3.6. *HR 1445*

The slight nebulosity associated with HR 1445 = HD 28929 is discernible only in the 8 and 24 μm bands, with a striated morphology evident at 8μm (Figure 15). The SED (Figure 16) does not reveal any infrared excess out to 24 μm and neither the star nor any nebular emission is seen at 70 and 160 μm.

HR 1445 is known as a peculiar star, an Hg-Mn main-sequence star of spectral type B8. Our spectral analysis also suggests a B8 (dwarf) star and we do see a weak Hg signature. The spectroscopic parallax distance is 136 ± 15 pc, and in good agreement with its Hipparcos parallax distance of 143 ± 17 pc. Walter & Boyd (1991) derived a spectroscopic parallax distance of 158 pc. From our χ^2 probability test, we deduce secure proper motion membership and HR 1445 also has a radial velocity consistent with that of Taurus. The good agreement of the distance, proper-motion, and radial velocity of this star with that expected for Taurus members provides strong support to the idea of HR 1445 being a Taurus member.

The age of this star, because it is main sequence, can be

constrained only to less than a few hundred Myr, within 1σ uncertainty. Westin (1985) quoted the age of this star as 60 Myr, in which case it would be an unlikely member of Taurus. HR 1445 is located toward a region of Taurus which is devoid of dense material along the line of sight. One might argue, to explain the nebulosity, that HR 1445 is located within a diffuse dust screen behind Taurus just like HD 29647. An alternate scenario is one in which star formation was active in Taurus several tens of Myr ago, when high-mass stars formed within a contraction time of a few Myr, while low mass stars formed a little later.

3.7. τ *Tau*

The τ Tau = HD 29763 region was not covered by any of the *Spitzer* surveys. However, examination of *WISE* image data reveals a compact, nebulous feature at 12 and 22 μm, similar to that observed for HR 1445. The SED (Figure 16) of τ Tau does not reveal any infrared excess out to 22 μm. The spectrum does not show the presence of any emission lines. Again, we can rule out the possibility that an accretion disk is present.

This source is a spectroscopic binary system composed of B and early A dwarfs (e.g. Cvetkovic & Ninkovic 2010). From our B3V spectral type we derive a spectroscopic parallax distance of 137 ± 9 pc. The Hipparcos parallax distance is 122 ± 13 pc. The value from Walter & Boyd (1991) is 142 pc. Both the proper motion and radial velocity of τ Tau are consistent with Taurus group V (as defined in Luhman et al. 2009), towards which it lies. Again, the only factor complicating the membership of this system with Taurus is its age. If it is a main-sequence star, as the spectrum indicates, then we can constrain its age as being $\lesssim 40$ Myr. Westin (1985) derived 20 Myr. However, in contrast to the later type B stars under consideration here, since the spectral type is so early τ Tau is plausibly coeval with the low mass T Tauri members of Taurus.

τ Tau also lies toward that region of Taurus which is devoid of dense material. A visual extinction of about 0.4 mag is derived. Only 1.6 degrees away from τ Tau is HP Tau/G2 which has had its distance accurately measured via VLBA at 161 pc, whereas we find 130 pc as the distance to the binary system; this would suggest a mainly line-of-sight separation of about 30 pc between the two stars. Indeed, HP Tau/G2 has higher reddening with $A_V = 2.6$ quoted by Rebull et al. (2010). We thus conclude the τ Tau is associated with the near side of the Taurus clouds.

3.8. *HD 31305 and AB Aur*

HD 31305 is not part of the area mapped under the guise of the *Spitzer* Taurus Legacy Survey, but it was covered in the "C2D" (PI N. Evans) maps. The source is not associated with nebulosity in any mid-infrared, near-infrared, or optical wavelength. However, it came to our attention through its proximity to known early-type member AB Aur. In the literature, HD 31305 mainly has been used as a reference star for variability studies of AB Aur and other nearby young stars, though itself turns out to be a variable (Cody et al. 2013). Its SED (Figure 16) shows some infrared excess in the near-to-far infrared and in section 4 we present a *DUSTY* model for the source.

We derive a spectral type of A1V for HD 31305, and a spectroscopic parallax distance of 174 ± 11 pc. Although this star lies at 1σ just outside the formal distance range that we consider for Taurus membership, (up to 162 pc), the star is seemingly a good candidate for membership. A secure proper-motion membership probability is found, but no radial velocity measurements exist. Keeping these points in mind, we conclude that HD 31305 is likely a newly appreciated member of Taurus.

AB Aur = HD 31293 is the prototypical Herbig Ae star with an assigned a spectral type of B9–A0e, consistent with our spectrum. It is a known member of Taurus with a Class II SED.

3.9. *HD 26212*

HD 26212 also lies outside the region of the *Spitzer* Taurus Legacy Survey, but was not covered in C2D. Inspection of DSS, 2MASS, WISE and IRAS images does not reveal any nebulosity towards this star. It does not have any infrared excess out to 24 μm as evidenced by its SED (Figure 16).

We arrived at a spectral classification of A5V for HD 26212. The corresponding spectroscopic parallax is 115 ± 4 pc which is in agreement (within the 2σ error) with both its larger Hipparcos parallax as well as the new Hipparcos reduction (van Leeuwen 2007) which yields a smaller value, $d_{HIP} = 100^{+7.8}_{-6.7}$. The proper motion of this star is consistent with Taurus, which means that it is tangentially comoving with the members of this cloud. The mean radial velocity quoted in literature is about 20 km s^{-1}, and within 1σ, agrees with that observed for Taurus members. The derivation of spectroscopic parallax yielded a visual reddening of $A_V = 0.16$. The low reddening and near distance suggests that HD 26212 lies in the outskirts of the L1498 region in Taurus. Since its spectrum suggests a main-sequence star and the spectral type is late, we can not meaningfully constrain the age.

3.10. *HD 27659, HD 283815*

Both of these stars are listed as having spectral type A0 and as probable members of Taurus based on infrared excess by Rebull et al. (2010).

The multiwavelength image cutouts of HD 27659 show extended emission at 8μm. The object is seen to be fuzzy but somewhat compact beyond this wavelength, a feature which is similar to multi-wavelength image morphology of HR 1445 and τ Tau. HD 27659 also shows considerable infrared excess beyond 25 μm (Figure 16). Rebull et al. (2010) find a Class II SED with $L_{IR}/L_{total} = 6 \times 10^{-4}$. Kenyon et al. (1994) classified HD 27659 as an A4V star and derived a spectroscopic parallax distance of $d = 146$ pc. Belikov et al. (2002) list HD 27659 as a member of the Perseus OB2 star forming complex, but its proper motion renders this improbable.

For HD 283815, there is no associated infrared nebulosity but Rebull et al. (2010) found the 8 μm to 24 μm flux ratio to indicate a Class III SED exhibiting a weak infrared excess, though this is not readily apparent from examination of the SED (Figure 16). There is sparse literature for HD 283815.

In terms of spectroscopic parallax, HD 27659 has an implied distance based on our derivation of an A3 spectral type of 164 pc which matches our criteria of membership with Taurus. For HD 283815 we did not obtain a spectrum, but using the literature spectral type of A0 shows that it does not meet our distance criteria, as can be discerned from the underluminous SED of Figure 16 when a 140 pc distance is assumed. In proper motion, however, the inverse is true with HD 27659 showing proper motion inconsistent with Taurus, but HD 283815 a high probability proper motion member. Radial velocity measurements exist for neither star.

Given the evidence, at present no strong statements can be made about the membership of either star. They could be early type members with peculiar motions, or background stars reddened due to the Taurus cloud. In both cases, there is some evidence for associated dust.

Of possible relevance is that lying only a quarter of a degree away from HD 27659 is HDE 283572, a Taurus member whose distance has been measured precisely by VLBA techniques. The implied distance between the two stars would be about 35 pc. From Figure 4, the proximity with a high surface density part of the cloud is evident and there is significant reddening implied for the further star HD 27659.

4. MODELLING THE DUST EMISSION WITH *DUSTY*

In this section we consider in more detail the nebular structures exhibited by the six early-type stars in Figures 10–15 and attempt to model the multiwavelength image morphology for several of the sources. Generally speaking, reflection nebulae appear bluish when illuminated by light from a nearby star on account of the scattering properties of dust. The star and the dust may be physically related, or the encounter between the star and a cloud of overdense interstellar medium may be by chance. A well-known example of the latter situation is the striated nebulosity associated with bright stars in the Pleiades. Infrared emission is also associated with the illuminated clouds, due to the warm dust, but compared to, e.g., H II regions, the infrared luminosity is lower and there is a lack of radio emission. The scattered-light images of Figure 1 and Figures 10–15 can be considered along with the SEDs in Figure 16 to classify the variety of physical scenarios among the sample.

The nebulae towards the embedded sources IC 2087-IR and V892 Tau are apparently the result of complex radiative transfer of an emitting source seen through a three-dimensional, non-uniform distribution of circumstellar dust that both obscures the central source and produces significant amounts of scattered light asymmetrically distributed with respect to the infrared point source. We do not attempt to model the emission from the disks and envelopes around these YSOs as such models appear elsewhere in the literature (e.g. Monnier et al. 2008). Conversely, HR 1445 and τ Tau (the latter based on WISE images since the source lies outside the area of the *Spitzer* map) show hints of nebulosity but no infrared excess; we also leave them out of the present modelling exercise because of the wide range of unconstrained parameter space allowed in the models. HD 27659 has just two data points within the region showing infrared excess, and we hesitate to attempt fitting of a unique function to it. HD 26212 and HD 283815 show neither significant infrared excess nor scattered light, and therefore cannot be modelled.

Below we model the dust surrounding 72 Tau, HD 29647, HD 282276 and HD 31305 as slabs, and make an attempt to reproduce their SEDs using the *DUSTY* code with results in Figure 18.

DUSTY takes the following input parameters: type of external radiation source, dust composition, grain size distribution, dust temperature at the edge nearest to the external source, geometry of the cloud (spherical shell / planar slab), density profile, and the optical depth. The dust temperature and optical depth together define the amount of radiation present at the edge of the photodissociation region. Ideally, given the dust properties and parameters of the illuminating star, the inner temperature of dust can be calculated giving us the separation from the star. Following Tielens (2005), we can calculate the dust temperature in a slab geometry as,

$$\begin{aligned}(T_d/Kelvin)^5 =& 2.7\times10^5\, G_0\, e^{-1.8\,A_V} \\ &+ 4.1\times10^{-4}\left[0.42-\ln(4.3\times10^{-4}\,G_0)\,G_0^{6/5}\right] \\ &+ 2.7^5 \end{aligned} \quad (4)$$

where A_V is the reddening caused by the slab. The assumption here is a simplistic model in which the absorption efficiency of the dust is directly proportional to the wavelength for $\lambda < \lambda_0 = 1000$ Å and is unity elsewhere; the dust size is $a = 1$ μm. G_0, the far-ultraviolet (FUV, $h\nu > 13.6$ eV) radiation field in terms of the average interstellar radiation field (1.6×10^{-3} erg cm^{-2} s^{-1}), is given by,

$$G_0 = 1.8\times\left(\frac{L_*}{100\,L\odot}\right)\left(\frac{\chi}{3.6\times10^{-4}}\right)\left(\frac{d}{0.02\ \mathrm{pc}}\right)^{-2} \quad (5)$$

where χ is the fraction of the star's luminosity (L_*) above 6 electronvolts and d is the distance from the star with the normalization constant that appropriate for a B8V star.

In the cases of interest here, the brightest part of the illuminated nebula is a few arcminutes wide, which, at a fiducial distance of 140 pc corresponds to ∼0.1 pc. For comparison, the H II region expected assuming a constant density pure hydrogen region with electron number density $n_e = 10^3$ cm^{-3} surrounding a B0V star is 0.4 pc (and would produce detectable radio emission) while for a B5V or B8V star the Strömgren radius, $\mathcal{R}_s$, is about 0.03 pc or 0.02 pc respectively (and usually would not be detectable in the radio). Note that $\mathcal{R}_s \propto n_e$, so local overdensities can allow the photodissociation regions (PDRs) to exist closer to the star thus heating them to higher temperatures. Therefore, if a dust slab were located at a few hundredths of a parsec from a B8 dwarf, the FUV radiation field it would experience is $G_0 \simeq 2$. Using $A_V \simeq 1$ for the slab, we then get $T_d \sim 10$ K. However, this over-simplified picture overlooks important processes within PDRs such as cooling through trace species such as [OI] and [CII], and the inhomogeneities in the dust cloud as indicated by the changing morphology of the nebulae towards the B stars with wavelength.

In our experiments with *DUSTY*, all conducted assuming a power-law grain size distribution according to the Mathis-

Rumpl-Nordsieck model (Mathis et al. 1977), we found the following general trends for a simulated dust slab. As the optical depth or the thickness of the slab is reduced toward zero, the scattered and thermal components of the output flux decrease, thus giving an output spectrum close to the input flux spectrum, as expected. As the dust temperature is lowered, there is an increase in the thermal emission peak relative to the primary (scattered stellar flux) peak. The thermal bump flattens and broadens if the relative abundance of amorphous carbon to graphite increases, whereas increasing the relative abundance of silicates produces the broad 10 and 18 μm features.

For 72 Tau, which we discussed above as a plausible Taurus member, we were able to reproduce the SED with *DUSTY* using the parameters: (i) $T_{\rm eff} = 12,500$ K blackbody as the external radiation source; (ii) dust composition such that silicates from Draine & Lee (1984) and amorphous carbon from Hanner (1988) are in a ratio of 1:4 (however, the output not very sensitive to this ratio so long as silicate fraction is less than 1); (iii) a 40 K dust temperature at the edge nearest to the external source; (iv) a 0.55 μm optical depth of 0.1 (corresponding to $A_V \simeq 0.1$). The resultant ratio of the dust contribution to the observed flux of the central star, a B7V-type blackbody, is about 1:200. This final model of the SED is shown in Figure 18. Since the fraction of the observed flux contributed by dust emission is much less compared to that contributed by the central star itself, we conclude that the nebula is not a photodissociation region, and we do not expect any free-free emission (indicative of an ionizing front) from it.

Moving on to HD 29647, we argued above that this source is probably not associated with Taurus since it is somewhat distant at 160–180 pc and does not appear to be comoving with the members of this cloud. However, it does illuminate nebulosity and has a substantial infrared excess. We see on inspection of the SED that there is a broad silicate feature evident at 10μm, and another thermal bump at about 60μm. On modelling this emission with *DUSTY*, we find that two dust components are required to explain this. One produces the broad silicate feature, requiring dust temperature at the inner boundary between 400 and 4500 K. The cooler limit comes from a fit to the thermal bump of the dust continuum emission. The hotter temperature limit is defined by the fit of the SED to optical data points. Clearly, any dust temperature beyond $\sim$ 1400 K is unphysical in this case, keeping in mind the environment of a B9III star. In our dust model we assume somewhat arbitrarily a 500 K temperature but the use of different temperatures within the range specified above does not affect the overall fit substantially. The second dust component is characterized by a temperature of about 45 K, which is defined by the peak of the thermal bump seen at tens of microns. To reproduce the SED as shown in Figure 18 we used (i) a blackbody with $T_{\rm eff} = 10,900$ K as the external radiation source; (ii) dust composition of silicates from Draine & Lee (1984) (with the output not very sensitive to the composition); (iii) dust temperature at the edge nearest to the external source: 500 K for slab A and 46.5 K for slab B; (iv) optical depth of 0.1 and 4 at 0.55μm for slabs A and B respectively (we need $\tau_A + \tau_B \simeq 4$, so that the total A_V for this star equals about 3.6). The output from slab A was passed as input to slab B and thus the overall output was calculated. To the output of slab B, another contribution from the output of slab A had to be added (in a 1:10 ratio) to the result of *DUSTY* in order to reproduce the observed flux,

Turning to HD 282276, the star seems to be a distant source (422 ± 52 pc) relative to Taurus, perhaps instead related to the Perseus cloud. Yet it still produces both a nebula and a thermal excess. The $\sim$ 3 arcmin-wide size of the nebula corresponds to a roughly 0.4 pc diameter structure at 420 pc. The H II region for a B8V star surrounded by a pure-hydrogen nebula would be about 0.02 pc in diameter and as the two values are inconsistent (even if our distance estimate is wrong by a factor of 3), we believe that the nebula is not a PDR immediately surrounding the H II region. The SED shows two bumps in the infrared, indicative of contribution from two different dust components. We can reproduce this SED with *DUSTY* using the parameters for slab A: (i) a blackbody with $T_{\rm eff} =$ 11,400 K as the external radiation source; (ii) silicate grains from Draine & Lee (1984); (iii) a 200 K dust temperature at the edge nearest to the external source; (iv) a 0.55 μm optical depth of 1.4. The output of slab A summed with a 6:1 contribution from the star (blackbody) was fed into slab B, which was modeled to have the same dust composition and grain-size distribution of slab A, and a dust temperature as 35 K at the edge, with visual optical depth of 1.6. Together, the optical depth adds up to three, corresponding to $A_V \simeq 2.8$, approximately the average extinction through the Taurus dark cloud. The dust composition is only suggestive; the bump at 10μm is much too broad to guess the silicon abundance. However, noting that the increase of amorphous carbon abundance relative to silicon results in a broad spectral feature at $\sim 0.12\mu$m and flattening of the thermal bump, we expect the relative amorphous carbon content to be small. Also, this broad bump makes it difficult to interpret the temperature of slab A, and we note that the edge temperature for this slab can lie anywhere between 100 and 300 K.

HD 31305 is an A1V star with very little reddening ($A_V \simeq 0.1$), proper motion consistent with Taurus, but lying somewhere between 165–185 pc. There is no nebulosity apparent but the SED shows infrared excess in the near-to-far infrared. Investigation of its SED relative to a range of *DUSTY* models tells us that the 10 μm silicate feature is probably strong, above the blackbody line, with the second thermal bump at a longer wavelengths broad and flat. This SED morphology indicates a similar abundance of silicon and amorphous carbon. The silicate feature remains significant if the edge temperature of the dust slab is set to lie between 100 and 500 K, but this is also dependent on the optical depth. We model this SED using the following parameters for a single slab. (i) blackbody with $T_{\rm eff} =$ 9,400 K (=A1V) as the external radiation source; (ii) silicate and graphite grains from Draine & Lee (1984) in a 10:1 ratio; (iii) a 350 K dust temperature at the edge nearest to the external source; (iv) 0.55 μm optical depth of 0.05. The contribution of the central star relative to the thermal and scattered dust emission is 4:1. The dust emission could equivalently be modeled using a 2-slab model to get a better fit, but based on the inspection of 2MASS cutouts (and also from the

low reddening value) of this star, we do not expect a 2-slab scenario.

5. SUMMARY & CONCLUSION

Early-type stars illuminating infrared nebulae found in *Spitzer* IRAC/MIPS maps of the Taurus-Auriga Molecular Cloud complex led us to carry out a more comprehensive search for early-type stars in this star-forming region. We compiled a list of 329 candidate early-type stars (see Table 3) towards Taurus from (i) previously-known O, B stars listed by SIMBAD, (ii) proposed B stars from Rebull et al. selected to have infrared excess and followed up spectroscopically, (iii) stars from the *Two Micron All Sky Survey* Point Source Catalog selected on the basis of photometric color, and (iv) early-type stars spectroscopically identified in the *Sloan Digital Sky Survey*. This set of stars was then tested against various membership criteria including distance, kinematics, and age criteria.

First, we provided accurate spectral type information for about 20 stars which were spectroscopically followed up from our initial sample at the 200-inch Hale telescope at the Palomar Observatory. This, along with the magnitudes available in literature has helped in deriving spectroscopic parallax distances to the stars, accounting for extinction. Notably, the presence of several diffuse interstellar bands is well-correlated with the estimated distances; none of the stars we believe associated based on distance or kinematic arguments with the Taurus star forming region exhibit these features, seen in only more distant stars. Several of the spectra show emission lines which in two cases are associated with known young stellar objects and in the other two cases appear associated with background Be stars also exhibiting infrared excesses.

Hipparcos parallaxes and spectroscopic parallaxes were used to select stars between 128 and 162 pc, allowing for error. Proper motion membership was tested by calculating the χ^2 probability using the proper motion of various comoving groups in Taurus (defined by Luhman et al. 2009). Radial velocity, wherever available, has been compared with that of the previously-known members of Taurus. We have also specially considered all early-type sources illuminating nebulae, regardless of whether they meet the distance and kinematic criteria.

Our final assessment of membership is shown in Table 6. Through this work, we have found three stars of spectral type B, and two of spectral type A to be newly-appreciated members of Taurus. Specifically, HR 1445 (HD 28929), τ Tau (HD 29763), 72 Tau (HD 28149), HD 31305, HD 26212 meet the kinematic and distance criteria while HD 27659, and HD 283815 show ambiguous kinematic and/or distance properties that make their membership plausible but not secure. Additional or improved space velocity information for these and several other stars could confirm their membership. These sources should be considered along with the currently accepted early-type members: IC2087-IR (B5-like luminosity but heavily self-embedded source with a continuum-emission optical and infrared spectrum), the binary system V892 Tau (Elias 1; a B8-A6 self-embedded Herbig Ae/Be star with

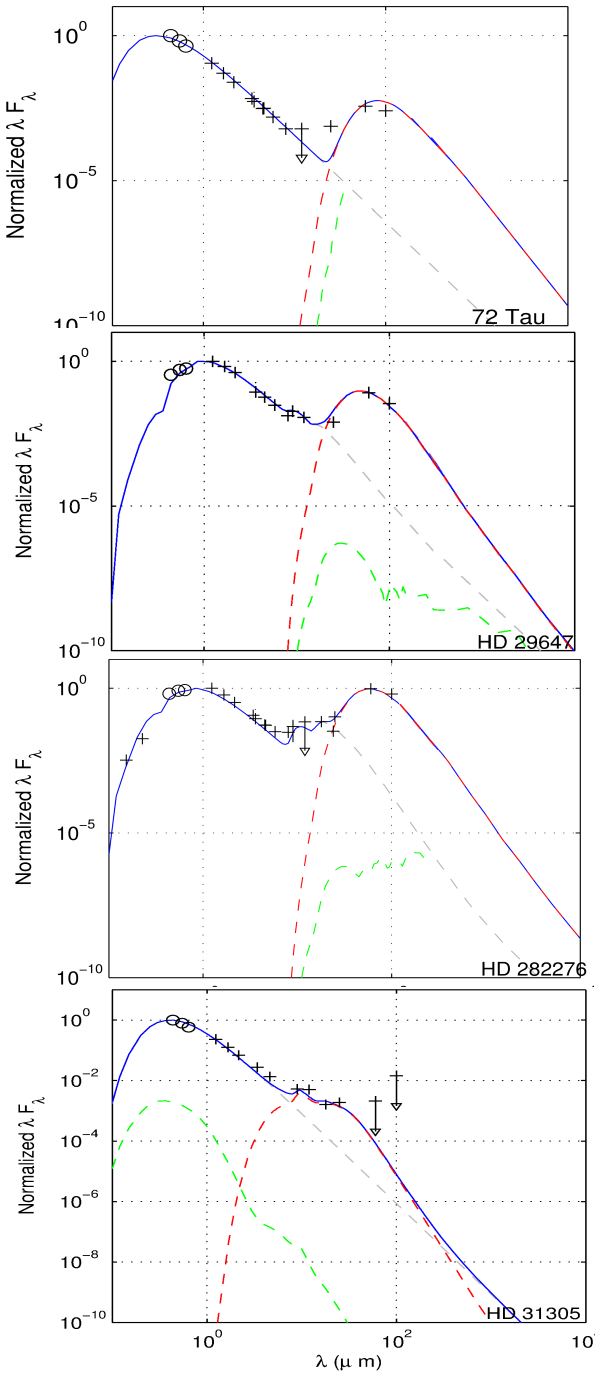

Figure 18. Modelling the SEDs (black data points) of some sources having far-infrared excess using *DUSTY*. For each of the sources, the attenuated blackbody representing the star is the grey dashed line, the contribution from the thermal and scattered emission components from the associated dust slab are shown as red and green dashed lines, respectively, and the blue solid line represents the total model output. Photometric points with error bars are shown; the circles represent BVR photometry that is reported without errors. *72 Tau*: A dust slab having 40 K temperature at the boundary closest to 72 Tau roughly reproduces the SED. *HD 29647 Tau*: Two slab components are required to reproduce the SED, one chosen to have a dust temperature of 500 K to reproduce the 10μm silicate feature, and another one at about 45 K. *HD 282276*: Two dust slabs, having inner-edge temperatures of 200 K and 35 K are required to faithfully reproduce the SED. *HD 31305*: The inner-edge dust temperature was found to be 350 K.

a near-equal brightness companion), the triple system HD 28867 (B8 +2×B9.5), AB Aur (A0e, a Herbig Ae/Be star), and HD 31648 (MWC 480; A2e, another Herbig Ae/Be star). While HD 28867 is located to the south of the main Taurus-Auriga clouds and therefore not recovered in our search, the other known early type members were recovered, although to varying degrees of security. Notably, more than half – but not all – of the stars listed above distinguish themselves through illumination of optical or infrared nebulae. Furthermore, two-thirds – but not all – of the stars have mid-infrared excesses which may be due to an extended nebula or to a more compact protoplanetary or later stage debris disk.

Among the stars with infrared reflection/scattered-light nebulae, three sources (HD 282276, HD 28149 = 72 Tau, and HD 29647) have been used as intrinsically bright background "candles" in studies of the molecular cloud's physical and chemical properties. Our analysis shows, however, that HD 282276 (the northernmost circled source in Figure 1) is likely a B-type star lying background to Taurus and close to the distance of the Perseus star-forming region, although well east of it. The molecular material may also be at that further distance. In the case of 72 Tau the kinematics and distance are both consistent with those of previously-known members of Taurus. While chance superposition with the Taurus cloud is possible this main-sequence star was probably born near its present environment and is truly associated with the cloud, unlike the case of the stars in the older Pleiades. Our assessment of HD 29647 suggests an object at similar distance but having different kinematics. Both HD 29647 and 72 Tau have nebulae which appear to be morphologically similar to the striated nebulosity toward the Pleiades stars Merope and Maia. The difference is that the Taurus nebulae under study here are much fainter and much less distinct at visible wavelengths than the Pleiades cases, possibly due to the amount of foreground extinction or to the spectrum of incident radiation (and less likely due to the dust properties).

We modelled the nebular dust emission of a subset of interesting stars also showing infrared excess. The dust temperatures found via this study, which account for the thermal dust emission peaks in the SEDs, are usually about 45 K. In some cases (viz. HD 282276 and HD 29647) there is evidence of two dust components contributing to the infrared emission, where the higher-temperature component is between 100 K and 500 K. The distance between the nebulae and the early-type stars can be estimated by balancing the heating and cooling rates. However, the unknown composition, complicated morphology and the self-similar nature of the radiation transfer makes the problem very challenging. Nevertheless, the infrared excess tells us that the star is sufficiently close to the nebula so as to heat it. Kinematic information of the stars supplement this proximity information to help distinguish between association with the cloud and chance superposition

We thank John Carpenter, Varun Bhalerao, and Eric Mamajek for their various suggestions and helpful advice. This research has made use of the DUSTY code developed by Gary Ferland, IRAF distributed by the National Optical Astronomy Observatories, which are operated by the Association of Universities for Research in Astronomy, Inc., under cooperative agreement with the National Science Foundation, and the SIMBAD and VizieR online database services.

Spitzer, 2MASS, SDSS, WISE, Palomar 200-inch

REFERENCES

Abazajian, K. N., et al. 2009, ApJS, 182, 543
Abt, H. A., Levato, H., & Grosso, M. 2002, ApJ, 573, 359
Andrews, S. M., & Williams, J. P. 2005, ApJ, 631, 1134
Bally, J., Walawender, J., & Reipurth, B. 2012, AJ, 144, 143
Belikov, A. N., Kharchenko, N. V., Piskunov, A. E., Schilbach, E., & Scholz, R.-D. 2002, A&A, 387, 117
Blaauw, A. 1956, ApJ, 123, 408
Cardelli, J. A., Clayton, G. C., & Mathis, J. S. 1989, ApJ, 345, 245
Carpenter, J. M. 2001, AJ, 121, 2851
Carroll, B. W., & Ostlie, D. A. 2006, An introduction to modern astrophysics, 2e., ed. Carroll, B. W. & Ostlie, D. A.
Cernicharo, J., & Bachiller, R. 1984, A&AS, 58, 327
Cody, A. M., Tayar, J., Hillenbrand, L. A., Matthews, J., & Kallinger, T. 2013, AJ, 145, 79
Cvetkovic, Z., & Ninkovic, S. 2010, Serbian Astronomical Journal, 180, 71
de Zeeuw, P. T., Hoogerwerf, R., de Bruijne, J. H. J., Brown, A. G. A., & Blaauw, A. 1999, AJ, 117, 354
Didelon, P. 1982, A&AS, 50, 199
Dobashi, K., Uehara, H., Kandori, R., Sakurai, T., Kaiden, M., Umemoto, T., & Sato, F. 2005, PASJ, 57, 1
Draine, B. T., & Lee, H. M. 1984, ApJ, 285, 89
Elias, J. H. 1978, ApJ, 224, 857
Finkbeiner, D. P., et al. 2004, AJ, 128, 2577
Frerking, M. A., Langer, W. D., & Wilson, R. W. 1982, ApJ, 262, 590
Furlan, E., et al. 2008, ApJS, 176, 184
Girardi, L., Bertelli, G., Bressan, A., Chiosi, C., Groenewegen, M. A. T., Marigo, P., Salasnich, B., & Weiss, A. 2002, A&A, 391, 195
Goldsmith, P. F., Heyer, M., Narayanan, G., Snell, R., Li, D., & Brunt, C. 2008, ApJ, 680, 428
Gontcharov, G. A. 2006, Astronomy Letters, 32, 759
Güdel, M., Padgett, D. L., & Dougados, C. 2007, Protostars and Planets V, 329
Hanner, M. 1988, Grain optical properties, Tech. rep.
Hartmann, L., Stauffer, J. R., Kenyon, S. J., & Jones, B. F. 1991, AJ, 101, 1050
Herbig, G. H. 1960, ApJS, 4, 337
Hillenbrand, L. A., Knapp, G. R., Padgett, D. L., Rebull, L. M., & McGehee, P. M. 2012, AJ, 143, 37
Johnson, H. L. 1966, ARA&A, 4, 193
Kalas, P., Graham, J. R., Beckwith, S. V. W., Jewitt, D. C., & Lloyd, J. P. 2002, ApJ, 567, 999
Kenyon, S. J., Dobrzycka, D., & Hartmann, L. 1994, AJ, 108, 1872
Kenyon, S. J., Gómez, M., & Whitney, B. A. 2008, in Handbook of Star Forming Regions, Volume I, ed. Reipurth, B., 405–+
Kharchenko, N. V., & Roeser, S. 2009, VizieR Online Data Catalog, 1280, 0
Kharchenko, N. V., Scholz, R., Piskunov, A. E., Röser, S., & Schilbach, E. 2007, Astronomische Nachrichten, 328, 889
Kirk, H., & Myers, P. C. 2011, ApJ, 727, 64
Knapp, G. R., Finkbeiner, D. P., Padmanabhan, N., & Schegel, D. J. 2007, in Bulletin of the American Astronomical Society, Vol. 38, Bulletin of the American Astronomical Society, 781–+
Koornneef, J. 1983, A&A, 128, 84
Kraus, A. L., & Hillenbrand, L. A. 2007, AJ, 134, 2340
Kraus, A. L., Ireland, M. J., Martinache, F., & Hillenbrand, L. A. 2011, ApJ, 731, 8
Lesh, J. R. 1968, ApJS, 17, 371
Loinard, L., Torres, R. M., Mioduszewski, A. J., Rodríguez, L. F., González-Lópezlira, R. A., Lachaume, R., Vázquez, V., & González, E. 2007, ApJ, 671, 546
Lombardi, M., Lada, C. J., & Alves, J. 2010, A&A, 512, A67
Luhman, K. L., Allen, P. R., Espaillat, C., Hartmann, L., & Calvet, N. 2010, ApJS, 186, 111
Luhman, K. L., Mamajek, E. E., Allen, P. R., & Cruz, K. L. 2009, ApJ, 703, 399
Maheswar, G., Lee, C. W., Bhatt, H. C., Mallik, S. V., & Dib, S. 2010, A&A, 509, A44
Mathis, J. S., Rumpl, W., & Nordsieck, K. H. 1977, ApJ, 217, 425
Miller, G. E., & Scalo, J. M. 1979, ApJS, 41, 513

Table 1
Number of O,B stars known to SIMBAD towards Taurus (central rectangle) and neighboring regions of equivalent area in coordinates of Galactic latitude and Galactic longitude.

0°				
	304	513	342	
-10°				
	100	117	122	
-20°				
	32	46	33	
-30°				
	195°	180°	165°	150°

Monnier, J. D., Tannirkulam, A., Tuthill, P. G., Ireland, M., Cohen, R., Danchi, W. C., & Baron, F. 2008, ApJ, 681, L97
Morgan, W. W., Keenan, P. C., & Kellman, E. 1943, An atlas of stellar spectra, with an outline of spectral classification, ed. Morgan, W. W., Keenan, P. C., & Kellman, E.
Munari, U., Sordo, R., Castelli, F., & Zwitter, T. 2005, A&A, 442, 1127
Narayanan, G., Heyer, M. H., Brunt, C., Goldsmith, P. F., Snell, R., & Li, D. 2008, ApJS, 177, 341
Narayanan, G., Snell, R., & Bemis, A. 2012, MNRAS, 425, 2641
Palmeirim, P., et al. 2013, A&A, 550, A38
Parker, R. J., Bouvier, J., Goodwin, S. P., Moraux, E., Allison, R. J., Guieu, S., & Güdel, M. 2011, MNRAS, 412, 2489
Perryman, M. A. C., & ESA, eds. 1997, ESA Special Publication, Vol. 1200, The HIPPARCOS and TYCHO catalogues. Astrometric and photometric star catalogues derived from the ESA HIPPARCOS Space Astrometry Mission
Rebull, L. M., et al. 2010, ApJS, 186, 259
—. 2011, ArXiv e-prints
Rieke, G. H., & Lebofsky, M. J. 1985, ApJ, 288, 618
Roeser, S., Demleitner, M., & Schilbach, E. 2010, AJ, 139, 2440
Schmidt-Kaler, T. 1982, The Physical Parameters of the Star, ed. K. Schaifers & H. H. Voigt
Shuping, R. Y., Chiar, J. E., Snow, T. P., & Kerr, T. 2001, ApJ, 547, L161
Skrutskie, M. F., Cutri, R. M., Stiening, R., & Weinberg, M. D. e. a. 2006, AJ, 131, 1163
Smith, K. W., Balega, Y. Y., Duschl, W. J., Hofmann, K.-H., Lachaume, R., Preibisch, T., Schertl, D., & Weigelt, G. 2005, A&A, 431, 307
Takita, S., Kataza, H., Kitamura, Y., Ishihara, D., Ita, Y., Oyabu, S., & Ueno, M. 2010, A&A, 519, A83+
Tielens, A. G. G. M. 2005, The Physics and Chemistry of the Interstellar Medium, ed. Tielens, A. G. G. M.
Torres, R. M., Loinard, L., Mioduszewski, A. J., Boden, A. F., Franco-Hernández, R., Vlemmings, W. H. T., & Rodríguez, L. F. 2012, ApJ, 747, 18
Torres, R. M., Loinard, L., Mioduszewski, A. J., & Rodríguez, L. F. 2007, ApJ, 671, 1813
—. 2009, ApJ, 698, 242
Ungerechts, H., & Thaddeus, P. 1987, ApJS, 63, 645
van Leeuwen, F. 2007, A&A, 474, 653
Walter, F. M., & Boyd, W. T. 1991, ApJ, 370, 318
Walter, F. M., Brown, A., Mathieu, R. D., Myers, P. C., & Vrba, F. J. 1988, AJ, 96, 297
Westin, T. N. G. 1985, A&AS, 60, 99
White, R. J., & Hillenbrand, L. A. 2004, ApJ, 616, 998
Whittet, D. C. B., Shenoy, S. S., Clayton, G. C., & Gordon, K. D. 2004, ApJ, 602, 291
Zacharias, N., Monet, D. G., Levine, S. E., Urban, S. E., Gaume, R., & Wycoff, G. L. 2005, VizieR Online Data Catalog, 1297, 0

Table 2
Distances to known Taurus members measured through VLBI techniques.

Star	α_{J2000} (h,m,s)	δ_{J2000} (°,′,″)	Distance (pc)	Ref.
HDE 283572	04 21 58.847	28 18 06.51	128.5 ± 0.6	1
V773 Tau	04 14 12.922	28 12 12.30	131.4 ± 2.4	2
V1023 Tau (Hubble 4)	04 18 47.037	28 20 07.32	132.8 ± 0.5	1
T Tau	04 21 59.434	19 32 06.42	146.7 ± 0.6	3
HP Tau/G2	04 35 54.152	22 54 13.46	161.4 ± 0.9	4

Refs: (1) Torres et al. (2007), (2) Torres et al. (2012), (3) Loinard et al. (2007), (4) Torres et al. (2009)

Table 3

List of candidate early-type stars. The table is divided into sections, each compiled from a different selection source, as described in the text. The last three columns state whether or not (Y/N) the star is a probable Taurus member based on two distance estimates (d), proper motion (μ), and radial velocity(RV); see text. Error on $d_{\rm SPEC}$ is the standard deviation of distances calculated here using B,V,R,J,H, and K magnitudes.

B#	Star	α (ICRS 2000, degrees)	δ	$d_{\rm HIP}$	$d_{\rm SPEC}$ (pc)	$\mu_\alpha cos\delta$ (mas/yr)	μ_δ	RV (km s^{-1})	SpT	Candidate? d	μ/RV
					O,B, and A0 stars from SIMBAD						
1	HD 25063	60.036389	29.710836		195 ± 5	3.7 ± 0.9	-6.2 ± 0.8		B9	N	N/?
2	HD 25201	60.236744	23.201484	332^{+274}_{-103}	189 ± 5	-34.6 ± 15.2	-9.2 ± 15.2	13.8 ± 1.1	B9V	N/N	N/Y
3	HD 281490	60.871667	30.970278		792 ± 123	13.0 ± 1.6	-7.3 ± 1.7		B9/A3	N	N/?
4	BD+23 607	60.936736	23.620942		643 ± 94	5.1 ± 1.3	-9.7 ± 1.3		A0V	N	N/?
5	HD 25487	60.976316	28.125973	301^{+153}_{-76}	342 ± 32	1.9 ± 1.7	-18.1 ± 1.5		B8Ve+K0IV	N/N	Y/?
6	HD 283304	61.226290	27.545890		739 ± 69	-2.7 ± 1.3	-2.2 ± 1.3		B8V Si	N	N/?
7	HD 284130	61.487807	23.241767		943 ± 20	-2.4 ± 1.0	5.4 ± 1.0		B8	N	N/?
8	HD 283363	61.780708	28.560528		528 ± 25	6.4 ± 1.5	-7.6 ± 1.6		B9	N	N/?
9	HD 281679	62.320792	30.775956	185^{+85}_{-44}	373 ± 11	-8.1 ± 1.5	3.6 ± 1.2		B8	Y/N	N/?
10	HD 284179	62.785610	22.825372		745 ± 41	-1.2 ± 1.2	-4.3 ± 1.2		B8	N	N/?
11	HD 283507	62.969714	24.837432		405 ± 18	-3.0 ± 1.2	-4.2 ± 1.3		B9	N	N/?
12	HD 283449	63.112000	27.876861		1613 ± 652	-2.3 ± 1.8	-4.8 ± 1.8		A0V	N	N/?
13	HD 26571	63.213520	22.413458	316^{+113}_{-66}	159 ± 1	-3.0 ± 0.5	-10.9 ± 0.5	9.3 ± 3	B8III	N/Y	N/Y
14	HD 281815	63.852452	29.365851		548 ± 57	1.0 ± 1.6	-10.9 ± 1.6		B8	N	N/?
15	HD 281818	64.079170	29.256597		749 ± 67	7.1 ± 1.3	-12.2 ± 1.3		B8	N	N/?
16	HD 284228	64.085078	23.841866		839 ± 32	13.5 ± 1.2	-6.0 ± 1.2		B5	N	N/?
17	HD 283553	64.488019	24.577938	248^{+122}_{-62}	465 ± 15	-0.8 ± 0.7	-7.9 ± 0.7		B8	N/N	N/?
18	HD 281920	64.569998	29.807023		777 ± 69	6.5 ± 1.2	-6.0 ± 1.0		B5	N	N/?
19	V892 Tau	64.669250	28.320972		1697 ± 1548	10.9 ± 5.1	-29.7 ± 5.1		$\sim$A0V	Y:	Y/?
20	HD 27405	65.126585	25.827451	229^{+71}_{-44}	242 ± 5	6.7 ± 1.4	-5.2 ± 1.5		B9	N/N	N/?
21	HD 283567	65.137783	28.652376		655 ± 44	-2.0 ± 1.5	-4.9 ± 1.6		B9	N	N/?
22	HD 27638	65.645598	25.629314	82^{+7}_{-6}	104 ± 2	17.4 ± 2.0	-13.3 ± 1.9	15.3 ± 3.4	B9V	N/N	N/Y
23	HD 27778	65.999008	24.300992	223^{+73}_{-44}	238 ± 5	8.0 ± 1.5	-12.7 ± 1.5		B3V	N/N	N/?
24	HD 284427	66.341599	23.389317		577 ± 56	-5.5 ± 1.2	-4.4 ± 1.2		B9V	N	N/?
25	HD 28149	66.822698	22.996337	127^{+13}_{-11}	161 ± 3	0.4 ± 0.5	-14.4 ± 0.5	7.3 ± 2.6	B7V	Y/Y	Y/Y
26	HD 284479	67.311975	22.478510		1153 ± 158	2.6 ± 1.5	-6.9 ± 1.5		B8V	N	N/?
27	HD 282151	67.424917	30.684083		771 ± 15	-3.1 ± 1.6	-1.3 ± 1.6		B9V	N	N/?
28	HD 28482	67.593513	23.588859	301^{+110}_{-64}	204 ± 1	18.0 ± 0.6	0.5 ± 0.6		B8III	N/N	N/?
29	HD 284487	67.879371	22.220857		1102 ± 177	3.4 ± 1.4	-2.5 ± 1.4		B9V	N	N/?
30	HD 282240	68.022275	30.967710		824 ± 31	4.1 ± 1.3	-6.3 ± 1.4		B9V	N	N/?
31	HD 283677	68.045575	29.015574	344^{+248}_{-102}	541 ± 15	0.0 ± 0.8	-8.9 ± 0.7		B5V	N/N	N/?
32	CoKu HK Tau G1	68.173333	24.317778		5976 ± 4466	37.7 ± 4.5	-11.1 ± 4.5	20 ± 4.5	B2	N	N/Y
33	HD 282276	68.267637	29.363863		422 ± 52	2.0 ± 1.6	-12.5 ± 1.7		B8V	N	N/?
34	2MASS J04335319+2414080	68.471667	24.235583		1244 ± 177	3.7 ± 1.6	-1.4 ± 1.6		B8	N	N/?
35	HD 282278	68.585583	29.297556		439 ± 30	-2.3 ± 1.3	-3.4 ± 1.4		B9	N	N/?
36	HD 28929	68.658299	28.961151	143^{+20}_{-16}	157 ± 3	1.3 ± 2.2	-23.2 ± 2.0	12.6 ± 2.2	B8V Hg-Mn	Y/Y	Y/Y
37	HD 283701	68.729070	27.203107		307 ± 3	1.9 ± 1.3	-11.6 ± 1.3		B8III	N	N/?
38	2MASS J04353218+2427069	68.884125	24.451944		1104 ± 201	-1.8 ± 4.6	-4.4 ± 4.6		B8	N	N/?
39	HD 283740	69.260698	28.011207		778 ± 48	3.0 ± 1.5	2.4 ± 1.5		B8V	N	N/?
40	HD 29259	69.438853	30.407638	667^{+2782}_{-298}	312 ± 10	0.6 ± 1.0	-9.1 ± 0.8		B9	N/N	N/?
41	HD 282380	69.715330	30.449740		287 ± 50	-1.4 ± 1.5	-1.3 ± 1.5		B8	N	N/?
42	HD 284583	69.777811	22.712064		1017 ± 25	1.0 ± 1.3	-0.2 ± 1.3		B5	N	N/?
43	HD 29450	69.806437	22.652255	429^{+340}_{-132}	345 ± 11	0.9 ± 0.8	-1.3 ± 0.7	-10.9 ± 2.6	B9	N/N	N/N
44	JH 225	69.916538	25.342850		540 ± 125	-11.6 ± 4.6	-8.3 ± 4.6		B9	N	N/?
45	HD 283794	69.964024	27.188951		428 ± 12	5.1 ± 1.2	-8.4 ± 1.3		B9V	N	N/?
46	IC 2087	69.982292	25.750556			1.6 ± 5.9	-19.7 ± 5.9		B5	?	Y/?
47	HD 283772	70.246863	27.990404		519 ± 11	0.0 ± 1.3	-5.2 ± 1.3		B9V	N	N/?
48	HD 29647	70.283524	25.992765	177^{+43}_{-29}	160 ± 1	12.8 ± 0.9	-9.7 ± 0.7		B9III Hg-Mn	Y/Y	N/?
49	HD 29681	70.349520	22.676800		699 ± 18	0.4 ± 1.1	0.1 ± 1.1		B8V	N	N/?
50	HD 283809	70.353006	25.913469		695 ± 230	2.5 ± 1.6	-1.4 ± 1.7		B1.5V	N	N/?
51	HD 29763	70.561257	22.956926	123^{+13}_{-11}	137 ± 9	0.6 ± 0.2	-17.4 ± 0.2	12.3 ± 4.1	B3V	Y/Y	Y/Y
52	HD 283800	70.863805	27.026948		564 ± 42	1.3 ± 1.5	-9.1 ± 1.5		B8	N	N/?
53	HD 29935	70.975003	22.944410	90^{+11}_{-9}	175 ± 2	-0.5 ± 0.7	-15.8 ± 0.6	32 ± 4.8	A0V	N/N	Y/N
54	HD 283805	71.301213	26.453282		846 ± 17	-2.2 ± 1.4	-4.1 ± 1.4		B8V/A3	N	N/?
55	HD 30122	71.426948	23.627996	216^{+40}_{-29}	290 ± 1	9.8 ± 0.6	-17.3 ± 0.5	23.2 ± 2	B5III	N/N	Y/N
56	HD 282430	71.644099	30.615554		918 ± 97	-3.5 ± 1.7	-5.6 ± 1.7		B5	N	N/?
57	HD 282431	71.654007	30.404109		400 ± 16	5.1 ± 1.6	-9.5 ± 1.5		B9/A0	N	N/?

Table 3
List of candidate early-type stars. The table is divided into sections, each compiled from a different selection source, as described in the text. The last three columns state whether or not (Y/N) the star is a probable Taurus member based on two distance estimates (d), proper motion (μ), and radial velocity(RV); see text. Error on $d_{\rm SPEC}$ is the standard deviation of distances calculated here using B,V,R,J,H, and K magnitudes.

58	HD 282485	71.658884	29.317718		483 ± 16	4.1 ± 1.5	-5.6 ± 1.5		B9V	N	N/?
59	HD 283851	71.678804	27.261715		637 ± 46	-3.8 ± 1.2	-3.7 ± 1.2		B9V	N	N/?
60	HD 283836	71.729035	28.225371		336 ± 29	0.0 ± 1.3	-3.7 ± 1.3		B9	N	N/?
61	HD 283854	71.765792	26.765833		809 ± 29	-1.0 ± 1.4	-4.7 ± 1.4		B9V/A7	N	N/?
62	HD 283845	71.967880	27.744442		750 ± 23	2.9 ± 1.5	-4.7 ± 1.5		B3V	N	N/?
63	HD 30378	72.094763	29.773003	196^{+49}_{-33}	239 ± 5	6.1 ± 0.6	-25.6 ± 0.6	21.6 ± 3.5	B9.5V	N/N	Y/N
64	HD 30675	72.716687	28.314066	368^{+269}_{-109}	332 ± 11	7.2 ± 1.2	-16.6 ± 0.8		B3V	N/N	N/?
65	HD 283875	72.795560	25.622469		530 ± 63	2.1 ± 1.7	-1.7 ± 1.6		B8V	N	N/?
66	HD 282537	72.898060	30.021865		752 ± 16	-4.1 ± 1.6	-9.5 ± 1.6		B8	N	N/?
67	HD 283920	73.021685	26.917266		497 ± 3	-0.8 ± 1.7	-11.3 ± 1.7		B7III	N	N/?
68	HD 282548	73.297292	29.020944		999 ± 63	-4.7 ± 1.7	-3.4 ± 1.7		B9	N	N/?
69	HD 283952	73.318183	24.714376		765 ± 23	2.2 ± 1.3	-3.7 ± 1.3		B9V	N	N/?
70	HD 284874	73.364583	22.251722		793 ± 37	2.6 ± 1.0	-1.6 ± 1.0		B8	N	N/?
71	HD 31120	73.539369	23.066227		374 ± 28	-4.8 ± 1.1	-10.8 ± 1.1		B9V	N	N/?
72	HD 283932	73.677168	25.729056		442 ± 46	0.7 ± 1.5	-7.0 ± 1.4		B8V	N	N/?
73	HD 282653	73.945167	29.333056		670 ± 26	-4.4 ± 1.7	-9.3 ± 1.7		B9	N	N/?
74	HD 31353	74.029726	24.004623		294 ± 12	4.6 ± 1.2	-8.8 ± 1.3		B9	N	N/?
75	HD 282635	74.120904	29.994960	172^{+81}_{-42}	490 ± 21	2.0 ± 1.3	-5.4 ± 1.1		B8	Y/N	N/?
76	HD 282617	74.150050	30.882917		673 ± 51	-6.8 ± 1.7	-6.7 ± 1.7		B8	N	N/?
77	V722 Tau	74.205683	27.718514		2304 ± 583	1.0 ± 1.8	-2.6 ± 1.8		B3e	N	N/?
78	HD 283968	74.205773	24.043778		643 ± 103	2.3 ± 1.5	-1.9 ± 1.5		B9V	N	N/?
79	HD 284993	74.302100	22.159576		790 ± 44	2.4 ± 1.2	-3.9 ± 1.2		B9	N	N/?
80	HD 282633	74.362179	30.174772		581 ± 48	-2.4 ± 1.3	2.8 ± 1.3		B8V	N	N/?
81	HD 283971	74.382746	28.759850		859 ± 240	-3.5 ± 1.7	-5.4 ± 1.5		B9V	N	N/?
82	HD 284006	74.532658	26.298360		358 ± 30	-3.1 ± 1.5	-7.4 ± 1.4		B9	N	N/?
83	HD 282754	74.593708	29.722028		1033 ± 128	-1.0 ± 1.7	-2.3 ± 1.7		B9	N	N/?
84	BD+30 748	74.639620	30.697656		1202 ± 115	1.5 ± 1.3	-2.5 ± 1.3	7.2 ± 1.4	B1.5V	N	N/N
85	HD 284941	74.674310	23.585106		1011 ± 195	-0.1 ± 1.2	-3.5 ± 1.2		B9	N	N/?
86	HD 31679	74.719814	24.495712	379^{+498}_{-137}	378 ± 28	2.1 ± 0.9	-4.4 ± 0.8		B5	N/N	N/?
87	HD 284012	74.898442	25.807481	258^{+113}_{-60}	255 ± 26	0.7 ± 1.1	-7.3 ± 0.9	11 ± 2.5	B8	N/N	N/Y
88	HD 31806	74.973961	27.325604	138^{+52}_{-30}	232 ± 6	14.8 ± 1.6	-24.6 ± 1.7		B7V	Y/N	N/?
	Additional B and early A stars proposed by Rebull et al. 2010 from infrared excess										
89	HD 27659	65.727746	28.398614		164 ± 10	-23.7 ± 1.5	-17.8 ± 1.4		A3V	Y	N/?
90	HD 27923	66.329861	23.788020	194^{+101}_{-49}	277 ± 5	5.9 ± 1.1	-8.6 ± 1.1		B9V	Y/N	N/?
91	HD 283637	66.495250	27.617028		855 ± 279	-3.6 ± 1.7	-6.8 ± 1.7		B9.5V	N	N/?
92	2MASS J04285940+2736254	67.247550	27.607081		533 ± 75	1.7 ± 2.3	-15.5 ± 2.4		A4V	N	Y/?
93	2MASS J04313313+2928565	67.888075	29.482378		639 ± 144	-6.0 ± 5.1	0.3 ± 5.1		A1V	N	N/?
94	HD 284530	68.582858	23.447141		347 ± 9	7.1 ± 1.2	-15.5 ± 1.2		B9.5V	N	Y/?
95	HD 283751	69.353563	27.155458		1010 ± 85	6.1 ± 1.4	-1.9 ± 1.4		B5Ve	N	N/?
96	HD 283815	70.671592	24.688295		268 ± 40	8.7 ± 1.2	-20.4 ± 1.2		A0	N	Y/?
	Additional early type candidates selected from 2MASS photometry										
97	HD 25111	60.054439	23.149068			5.4 ± 1.1	-4.6 ± 1.1		A	?	N/?
98	HD 283286	60.959556	28.404501		420 ± 21	-6.9 ± 2.7	-5.19 ± 2.37		A2	N	N/?
99	04040178+2715454	61.007451	27.262593			-8.1 ± 5.6	-5.16 ± 4.98		?	?	N/?
100	HD 25554	61.160276	30.884204	207^{+70}_{-42}	280 ± 9	3 ± 1	1.97 ± 0.69		A0	N/N	N/?
101	HD 25620	61.208024	23.509276		176 ± 11	2.7 ± 1.1	-0.92 ± 1.01		F0	N	N/?
102	HD 25626	61.301075	27.609715	202^{+62}_{-38}	191 ± 3	16.7 ± 1	-26.23 ± 0.89	2 ± 1.8	A2	N/N	N/N
103	HD 25694	61.413234	28.395374		347 ± 15	1.6 ± 1.4	-5.01 ± 1.32		A0	N	N/?
104	04055962+2956381	61.498439	29.943959			0.1 ± 1.7	-5.63 ± 1.47		?	?	N/?
105	HD 283346	61.550881	25.362189		373 ± 32	5.7 ± 1.1	-9.94 ± 0.99		A2	N	N/?
106	HD 26212	62.432002	24.072944	123^{+17}_{-14}	115 ± 4	2.4 ± 0.8	-18.81 ± 0.55	20.3 ± 3.9	A5V	Y/N	Y/Y
107	HD 284189	62.614432	22.256375		289 ± 11	5.4 ± 1.1	-12.86 ± 1.02		A3	N	N/?
108	HD 284191	62.819075	22.248622		374 ± 30	3.6 ± 1.2	-10.64 ± 1.11		A0	N	N/?
109	HD 283467	62.988010	27.168309		648 ± 8	2.1 ± 1.5	-2.22 ± 1.33		A0	N	N/?
110	04115969+3046563	62.998756	30.782361			1.4 ± 1.7	-4.64 ± 1.46		?	?	N/?
111	04124695+2902138	63.195599	29.037144			0.7 ± 1.7	-1.05 ± 1.49		?	?	N/?
112	HD 283457	63.356642	27.357025			-3.9 ± 1.2	-6.57 ± 1.07			?	N/?
113	HD 283503	63.511797	24.813039		404 ± 68	3.2 ± 1.3	-17.16 ± 1.18		A7	N	Y/?
114	FM Tau	63.556610	28.213672		808 ± 710	4.7 ± 2.4	-29.78 ± 2.11		K3	Y	Y/?
115	CW Tau	63.570878	28.182714		236 ± 188	18 ± 5.1	-24.94 ± 4.5		K5V:e...	Y	Y/?
116	HD 281820	64.102354	29.149663			12.9 ± 1.6	-14.5 ± 1.48		A	?	N/?
117	04171672+2518050	64.319686	25.301403			-1.1 ± 2.3	-4.25 ± 2.08		?	?	N/?

Table 3
List of candidate early-type stars. The table is divided into sections, each compiled from a different selection source, as described in the text. The last three columns state whether or not (Y/N) the star is a probable Taurus member based on two distance estimates (d), proper motion (μ), and radial velocity(RV); see text. Error on $d_{\rm SPEC}$ is the standard deviation of distances calculated here using B,V,R,J,H, and K magnitudes.

118	DD Tau	64.629677	28.274725		396 ± 326	6.7 ± 5.1	-25.28 ± 4.49		K6V:e...	Y	Y/?
119	HD 284308	64.646193	22.701229		429 ± 40	1.6 ± 1.2	-5.07 ± 1.11		A3	N	N/?
120	FR Tau	64.897754	28.456022			5.9 ± 5.5	-25.32 ± 4.84			?	Y/?
121	HD 283568	65.094954	28.737826		688 ± 78	-5.9 ± 1.6	-6.58 ± 1.4		A0	N	N/?
122	HD 284383	65.391471	22.119671		684 ± 28	-2.9 ± 1.3	-2.22 ± 1.2		A0V	N	N/?
123	HD 283571	65.489190	28.443195	134^{+55}_{-30}	69 ± 29	9.1 ± 1.6	-25.94 ± 1.41	24.3 ± 1.9	F8V:e...	Y/N	Y/N
124	04233478+2804292	65.894960	28.074773			-8.8 ± 2.4	2.56 ± 2.12		?	?	N/?
125	FU Tau	65.897490	25.050747		118 ± 103	7.3 ± 4.5	-24.01 ± 4.08		M7.25	Y	Y/?
126	HD 27787	66.113276	30.124556		380 ± 33	-3 ± 1.5	-7.35 ± 1.3	-24	A0V	N	N/N
127	2MASS J04244457+2610141	66.185733	26.170592		254 ± 191	9.8 ± 4.5	-21.09 ± 4.04		M0	Y	Y/?
128	JH 15	66.209223	26.482108			-1 ± 2.2	-3.94 ± 1.97			?	N/?
129	04262631+2742225	66.609620	27.706273			3.8 ± 1.8	-3.9 ± 1.59		?	?	N/?
130	HD 283625	66.715248	28.953061		527 ± 16	1.1 ± 1.4	-5.86 ± 1.23		A1V	N	N/?
131	DG Tau	66.769586	26.104481			5.6 ± 1.7	-19.13 ± 1.53		GV:e...	?	Y/?
132	04273688+2936338	66.903701	29.609408			-4.6 ± 1.7	-5.56 ± 1.48		?	?	N/?
133	DH Tau	67.423219	26.549413		244 ± 198	9.3 ± 4.5	-21.56 ± 4.03		M0.5V:e	Y	Y/?
134	IQ Tau	67.464609	26.112596		88 ± 56	-2.2 ± 4.8	-16.88 ± 4.04		M2	Y	Y/?
135	DK Tau	67.684336	26.023512		76 ± 53	5.5 ± 2.4	-14.56 ± 2.16		M0V:e	Y	Y/?
136	2MASS J04305028+2300088	67.709603	23.002469			3.9 ± 4.5	-40.32 ± 4.14		F1	N	N/?
137	HD 28697	68.090832	25.185490	109^{+14}_{-11}	150 ± 2	-2 ± 0.6	-25.88 ± 0.54		A2	N/Y	N/?
138	HD 282267	68.099987	30.118652		342 ± 7	0.4 ± 1.5	-12.46 ± 1.38		A2V	N	N/?
139	HD 283688	68.108755	28.317406		145 ± 6	-3 ± 1.4	-10.39 ± 1.23		F5	Y	N/?
140	FZ Tau	68.132328	24.334158			1.6 ± 4.5	-27.61 ± 4.1			?	Y/?
141	HD 284484	68.192963	22.103749		287 ± 36	2.2 ± 1.5	-5.84 ± 1.39		A5	N	N/?
142	2MASS J04325030+2942395	68.209596	29.710960			1.2 ± 5.1	-2.52 ± 4.43			?	N/?
143	2MASS J04325316+2948046	68.221551	29.801318			-0.1 ± 6.7	-5.81 ± 5.81			?	N/?
144	HD 282270	68.275192	29.778140		294 ± 8	8 ± 1.6	-8.77 ± 1.39		A1V	N	N/?
145	HD 283718	68.366065	24.923085		693 ± 213	-5.5 ± 1.3	-2.9 ± 1.18		A3V/A0	N	N/?
146	GK Tau	68.394029	24.351647			10.7 ± 13.2	-1.55 ± 12.3		K7	N	Y/?
147	IS Tau	68.403326	26.163645		233 ± 158	11.9 ± 4.5	-22.53 ± 4.04		K7	Y	Y/?
148	DL Tau	68.412898	25.344065			2.4 ± 4.5	-12.74 ± 4.07		GV:e...	?	Y/?
149	HD 283684	68.570530	28.436188		392 ± 29	-5.7 ± 2.5	-6.68 ± 2.29		A7	N	N/?
150	HQ Tau	68.947255	22.839317			6.5 ± 4.5	-19.81 ± 4.15			?	Y/?
151	HP Tau	68.969924	22.906426		101 ± 79	-0.9 ± 10.3	-22.02 ± 9.49		K3	Y	Y/?
152	HD 282334	69.033170	30.394761		686 ± 66	-5.5 ± 1.4	-1.9 ± 1.21		A0	N	N/?
153	HD 29333	69.608312	29.387357	152^{+37}_{-25}	132 ± 7	3.7 ± 0.8	0.78 ± 0.7		A2	Y/Y	N/?
154	DO Tau	69.619111	26.180440			-7.1 ± 4.6	-29.61 ± 4.13		GV:e...	?	Y/?
155	HD 283739	69.682933	28.075829		251 ± 17	-4 ± 1.4	2.29 ± 1.24		A7	N	N/?
156	HD 282387	69.695646	29.475297		282 ± 59	5.7 ± 1.6	-11.32 ± 1.39		A0	N	N/?
157	GN Tau	69.837159	25.750568		138 ± 99	3.6 ± 4.6	-22.16 ± 4.14		M2.5	Y	Y/?
158	HD 283746	69.842850	27.765421		292 ± 8	-1.7 ± 1.4	-7.52 ± 1.33		A3	N	N/?
159	HD 29459	69.846455	25.218274	111^{+10}_{-9}	68 ± 3	18 ± 0.6	-10.68 ± 0.45	17.8 ± 3.1	A5Vn	N/N	N/Y
160	HD 29631	70.245274	23.939795			1.5 ± 1.1	-9.23 ± 1.1		F	?	N/?
161	HD 29646	70.332333	28.614989	103^{+10}_{-8}	82 ± 1	35.5 ± 0.3	-27.56 ± 0.44	25.3	A2V	N/N	N/N
162	04415107+2914109	70.462775	29.236408			-5.2 ± 1.7	-8.38 ± 1.48		?	?	N/?
163	HD 284648	70.572097	23.268516		428 ± 5	5.7 ± 0.9	-8.45 ± 0.83		A0	N	N/?
164	DP Tau	70.657043	25.260368		205 ± 133	-3.7 ± 5.1	-19.63 ± 4.61		M0V:e	Y	Y/?
165	04433905+2353578	70.912683	23.899431			-0.1 ± 1.5	-14.45 ± 1.37		?	?	Y/?
166	HD 282424	71.037023	30.866020			-1.4 ± 1.6	-9.18 ± 1.37			?	N/?
167	04454979+2442422	71.457514	24.711720			4.2 ± 2.3	-11.08 ± 2.09		?	?	N/?
168	HD 30168	71.550277	26.035498	266^{+104}_{-58}	166 ± 4	8.2 ± 0.7	-34.14 ± 0.63		A0	N/Y	N/?
169	HD 283868	71.778034	26.179319		16 ± 2	3.6 ± 1.4	-2.33 ± 1.26	30	K3pv/G6e	N	N/N
170	HD 283823	71.796194	28.964173		406 ± 51	3.8 ± 1.6	-12.6 ± 1.4		A2	N	N/?
171	HD 30309	71.865612	24.354856		398 ± 26	3 ± 1.4	-2.64 ± 1.28		A0/F5	N	N/?
172	HD 284763	71.940583	22.685857		458 ± 46	-2 ± 1.5	-1.48 ± 1.38		F0	N	N/?
173	DS Tau	71.952482	29.419766		98 ± 63	7.8 ± 2.7	-29.62 ± 2.35	0	K4V:e	Y	Y/N
174	HD 283861	71.975276	26.560652		463 ± 12	1.1 ± 1.5	-4.47 ± 1.43		A0	N	N/?
175	HD 30466	72.316676	29.571363	163^{+30}_{-22}	177 ± 5	8 ± 0.8	-28.18 ± 0.61	17	A0p	Y/N	N/Y
176	04492661+2730388	72.360927	27.510755			1.3 ± 1.4	-5.41 ± 1.24		?	?	N/?
177	HD 283842	72.548615	27.677257			-2 ± 1.7	-3.54 ± 1.51		A	?	N/?
178	HD 283830	72.585658	28.377142		675 ± 154	-3.1 ± 1.7	-12.58 ± 1.5		A2	N	N/?

Table 3
List of candidate early-type stars. The table is divided into sections, each compiled from a different selection source, as described in the text. The last three columns state whether or not (Y/N) the star is a probable Taurus member based on two distance estimates (d), proper motion (μ), and radial velocity(RV); see text. Error on $d_{\rm SPEC}$ is the standard deviation of distances calculated here using B,V,R,J,H, and K magnitudes.

179	HD 283885	72.743801	24.278521		343 ± 35	3.1 ± 1.5	-5.65 ± 1.37		A5	N	N/?
180	UY Aur	72.947410	30.787076		115 ± 44	4.9 ± 2.3	-19.24 ± 2.06	18 ± 3	G5V:e...	Y	Y/Y
181	HD 283945	73.028640	25.437055		515 ± 66	-4.4 ± 1.7	-8.31 ± 1.54		A2	N	N/?
182	HD 283889	73.110373	28.729730		592 ± 65	-3.2 ± 1.6	-6.75 ± 1.4		A0	N	N/?
183	BD+26 758	73.135736	27.027236		158 ± 12	-12.3 ± 1.5	-22.63 ± 1.34		A5	Y	N/?
184	HD 283890	73.185411	28.619612		301 ± 48	-1.4 ± 1.7	-4.83 ± 1.49		A3	N	N/?
185	HD 283941	73.289352	25.491105		487 ± 69	4.4 ± 1.5	-7.67 ± 1.44		A0	N	N/?
186	HD 283893	73.392339	28.456354		616 ± 88	-2.5 ± 1.4	-11.43 ± 1.23		A0	N	N/?
187	HD 284873	73.431141	22.178329			6.4 ± 1	-6.11 ± 0.93		A	?	N/?
188	HD 283911	73.731551	27.630496		411 ± 57	1.1 ± 1.5	-8.24 ± 1.33		A2	N	N/?
189	HD 31329	73.914289	22.187528		281 ± 17	-1.2 ± 0.9	-8.15 ± 0.93		A2	N	N/?
190	HD 282624	73.997451	30.567085	152^{+63}_{-34}	451 ± 1	5.4 ± 1.4	-20.32 ± 0.95	23.2 ± 2.8	G2III	Y/N	Y/N
191	HD 284989	74.128224	22.591051		775 ± 86	1.5 ± 1.4	-5.63 ± 1.38		A0	N	N/?
192	HD 31581	74.581425	29.847393		194 ± 9	-1.7 ± 1.5	-3.9 ± 1.21		A2	N	N/?
193	HD 31648	74.692775	29.843609	131^{+24}_{-18}	124 ± 32	5.6 ± 0.9	-21.16 ± 0.69		A3Ve/A2	Y/Y	Y/?
194	HD 284946	74.893341	23.502550		479 ± 21	-1.8 ± 1.2	-5.04 ± 1.1		A0	N	N/?
195	HD 284035	74.941567	24.314204		523 ± 61	-7 ± 5.9	-7.11 ± 5.65		A0	N	N/?
					O,B,A stars from Knapp et al. *SDSS* data						
196	04095167+2520112	62.465271	25.336500		4389 ± 605	-1.6 ± 3.7	-4.8 ± 3.7	-0.1 ± 1.6	A0	N	N/N
197	04111342+2447170	62.805889	24.788080		8576 ± 2737	0.3 ± 3.8	-3.3 ± 3.8	37.5 ± 3.2	A0	N	N/N
198	04113476+2524136	62.894859	25.403830		12774 ± 2784	-3.7 ± 4.3	-2.5 ± 4.3	-2.5 ± 2.5	A0	N	N/N
199	04122067+2430477	63.086201	24.513310		6397 ± 895	-2.0 ± 3.8	-3.9 ± 3.8	-7.4 ± 1.5	A0	N	N/N
200	04132281+2620282	63.345039	26.341200		11426 ± 1981	1.3 ± 4.2	-6.2 ± 4.2	-1.1 ± 1.7	A0	N	N/N
201	04135173+2631257	63.465488	26.523861		11234 ± 838	1.1 ± 4.4	-4.2 ± 4.4	69.9 ± 2.6	A0	N	N/N
202	04135440+2609097	63.476631	26.152700			3.2 ± 3.9	-9.9 ± 3.9	64.2 ± 2.7		?	N/N
203	04142194+2500478	63.591438	25.013350		8722 ± 1026	0.1 ± 4.3	-3.2 ± 4.3	-14.5 ± 3	A0	N	N/N
204	04142864+2608046	63.619362	26.134621		7392 ± 1367	3.0 ± 3.8	-8.2 ± 3.8	2.3 ± 1.8	A0	N	N/N
205	04152014+2629584	63.833901	26.499580		8897 ± 748	3.8 ± 4.1	-7.5 ± 4.1	25.6 ± 2.2	A0	N	N/N
206	04152167+2522393	63.840290	25.377581		18112 ± 1920	10.3 ± 4.4	-5.3 ± 4.4	101.5 ± 5.1	B6	N	N/N
207	04153610+2538570	63.900219	25.649200			7.4 ± 4.5	-0.3 ± 4.5	-66.4 ± 7.3	O	?	N/N
208	04154968+3035156	63.957008	30.587580		20128 ± 6470	4.7 ± 5.5	-0.5 ± 5.5	62.6 ± 3.7	A0p	N	N/N
209	04155589+2941428	63.982899	29.695271		14164 ± 7605	2.0 ± 4.4	2.7 ± 4.4	2.8 ± 2.6	A0	N	N/N
210	04160013+2730051	64.000603	27.501440		5608 ± 403	-0.9 ± 4.3	0.9 ± 4.3	110.4 ± 2.6	A0	N	N/N
211	04161037+3053487	64.043190	30.896900		14170 ± 5336	2.3 ± 4.6	-3.0 ± 4.6	-3 ± 2.3	A0	N	N/N
212	04162411+2434450	64.100487	24.579250		7766 ± 575	6.0 ± 3.9	-3.8 ± 3.9	21.9 ± 1.9	A0	N	N/N
213	04162961+2643589	64.123383	26.733021		10475 ± 1941	5.8 ± 4.0	-6.5 ± 4	31.8 ± 3.2	A0	N	N/N
214	04163672+2650392	64.152969	26.844250		11636 ± 1775	1.4 ± 4.4	-3.7 ± 4.4	0 ± 3	A0	N	N/N
215	04165196+2601449	64.216522	26.029141		12571 ± 2322	6.9 ± 4.3	-8.3 ± 4.3	26.8 ± 2.7	A0	N	N/N
216	04170011+2522475	64.250412	25.379850		5729 ± 756	4.1 ± 3.9	1.6 ± 3.9	-10 ± 2.8	A0	N	N/N
217	04170272+2644290	64.261322	26.741400		16618 ± 6674	-0.9 ± 4.2	-1.6 ± 4.2	-42 ± 1.9	A0	N	N/N
218	04174593+2618579	64.441330	26.316080		12914 ± 2916	11.6 ± 4.2	-6.2 ± 4.1	-23.7 ± 2.6	A0	N	N/N
219	04180495+2952363	64.520653	29.876770		5337 ± 739	0.4 ± 4.3	-1.0 ± 4.3	56.2 ± 2.9	A0	N	N/N
220	04180763+2846201	64.531853	28.772261			-3.0 ± 4.3	2.4 ± 4.3	-8.2 ± 4		?	N/N
221	04182140+2552023	64.589111	25.867371		13651 ± 2176	0.7 ± 4.5	-2.1 ± 4.5	19.9 ± 2.3	A0	N	N/Y
222	04182615+2454459	64.608917	24.912741		6099 ± 481	4.1 ± 3.9	-0.7 ± 3.9	23.2 ± 1.9	A0	N	N/N
223	04183386+2547250	64.641022	25.790310		7144 ± 1040	1.2 ± 3.9	-1.1 ± 3.9	40.5 ± 2	A0	N	N/N
224	04183552+3006115	64.647987	30.103270		11840 ± 6382	5.1 ± 4.2	-3.7 ± 4.2	-28.9 ± 1.6	A0	N	N/N
225	04183818+2735261	64.658989	27.590740		5840 ± 429	0.1 ± 4.3	-2.7 ± 4.3	93.5 ± 4.2	A0	N	N/N
226	04184109+2449442	64.671127	24.828951		6709 ± 1285	5.4 ± 3.9	-6.5 ± 3.9	-28.6 ± 3.2	A0	N	N/N
227	04184261+2550172	64.677528	25.838110		4135 ± 2695	4.5 ± 4.4	-1.5 ± 4.4	60.3 ± 2.2	A0	N	N/N
228	04185780+3004129	64.740830	30.070339		7548 ± 2854	-2.8 ± 4.2	-1.0 ± 4.2	16.4 ± 1.5	A0	N	N/Y
229	04185955+3050026	64.748200	30.834129		13418 ± 4181	-5.9 ± 4.7	-2.4 ± 4.7	17.3 ± 3.3	A0	N	N/Y
230	04190128+2918288	64.755364	29.308020		17037 ± 6908	0.3 ± 4.7	-0.9 ± 4.7	-42 ± 2.8	A0	N	N/N
231	04190952+2907266	64.789658	29.124069		10467 ± 2703	0.5 ± 4.4	-1.4 ± 4.4	-24.5 ± 2	A0	N	N/N
232	04191436+2552469	64.809807	25.879721		7069 ± 461	3.8 ± 3.9	-0.2 ± 3.9	22.5 ± 2.3	A0	N	N/N
233	04191985+2749395	64.832733	27.827740			-2.6 ± 4.3	-4.5 ± 4.3	37 ± 2.7		?	N/N
234	04192106+2931069	64.837784	29.518650		5810 ± 1609	0.1 ± 4.3	-4.8 ± 4.3	-67 ± 1.5	A0	N	N/N
235	04193853+2949396	64.910599	29.827740			-12.3 ± 5.8	-6.3 ± 5.8	-5.3 ± 2.2	0	?	N/N
236	04195512+2801576	64.979652	28.032820		20143 ± 8223	-4.1 ± 5.0	-13.7 ± 5	49.8 ± 5.6	B9	N	N/N
237	04200363+2950586	65.015122	29.849670		22508 ± 13749	-2.8 ± 4.4	1.1 ± 4.4	25.8 ± 3.4	A0	N	N/N
238	04200803+2843222	65.033478	28.722879		5852 ± 1409	-3.4 ± 4.3	-2.6 ± 4.3	13.5 ± 1.5	A0	N	N/Y
239	04203271+3015272	65.136299	30.257601		11597 ± 1905	2.5 ± 4.8	-5.1 ± 4.8	-15.5 ± 3.2	A0	N	N/N
240	04203551+2945073	65.147903	29.752081		6242 ± 572	-4.8 ± 4.4	-3.4 ± 4.4	-21.6 ± 1.3	A0	N	N/N
241	04204960+3010153	65.206642	30.170919		5912 ± 1380	4.0 ± 4.3	-3.2 ± 4.3	-1 ± 1.8	A0	N	N/N
242	04205096+2840119	65.212318	28.670050		5659 ± 1353	1.2 ± 4.3	-1.7 ± 4.3	1.5 ± 1.6	A0	N	N/N
243	04210068+2711172	65.252724	27.188320		15034 ± 10003	1.8 ± 3.8	-8.5 ± 3.8	-168.4 ± 2.2	A0	N	N/?

Table 3
List of candidate early-type stars. The table is divided into sections, each compiled from a different selection source, as described in the text. The last three columns state whether or not (Y/N) the star is a probable Taurus member based on two distance estimates (d), proper motion (μ), and radial velocity(RV); see text. Error on $d_{\rm SPEC}$ is the standard deviation of distances calculated here using B,V,R,J,H, and K magnitudes.

244	04210658+2546557	65.277359	25.782129	16067 ± 2065	-9.8 ± 4.1	-15.4 ± 4.1	64 ± 2.8	B6	N	N/N
245	04211397+2850064	65.308197	28.835079	12704 ± 3762	1.0 ± 4.7	3.1 ± 4.7	-45.6 ± 4	A0	N	N/N
246	04212796+3002107	65.366501	30.036320	6888 ± 1080	-4.7 ± 4.2	-2.8 ± 4.2	-33.4 ± 1.4	A0	N	N/N
247	04213150+2520399	65.381271	25.344431	4475 ± 673	2.7 ± 3.8	-3.2 ± 3.8	-11.3 ± 1.7	A0	N	N/N
248	04213151+2917334	65.381310	29.292620	9353 ± 1500	0.6 ± 4.5	-0.1 ± 4.5	-1.6 ± 1.9	A0	N	N/N
249	04213578+2936482	65.399117	29.613489	10898 ± 2482	-1.7 ± 4.5	-4.6 ± 4.5	-22.9 ± 2	A0	N	N/N
250	04222582+2616149	65.607529	26.271099	13098 ± 3069	-1.3 ± 4.5	-3.3 ± 4.5	-11.5 ± 2.7	A0	N	N/N
251	04224008+2957006	65.667023	29.950230	8232 ± 1932	-1.0 ± 4.4	1.4 ± 4.4	4.8 ± 1.7	A0	N	N/N
252	04224882+2904442	65.703377	29.079029	14458 ± 3048	0.1 ± 5.0	-4.6 ± 5	-1.4 ± 2.1	A0	N	N/N
253	04225306+2613188	65.721130	26.222340		-2.9 ± 4.4	-8.6 ± 4.4	-28.4 ± 4.3	0	?	N/N
254	04225686+2939043	65.736900	29.651279	9610 ± 1149	-6.2 ± 4.6	2.3 ± 4.6	20 ± 2.1	A0	N	N/Y
255	04230562+2538494	65.773392	25.647060	5550 ± 424	2.4 ± 3.8	-0.2 ± 3.8	1.9 ± 2.4	A0	N	N/N
256	04231596+2941221	65.816551	29.689520	9546 ± 1035	8.9 ± 4.7	-8.6 ± 4.7	57.1 ± 2.4	A0	N	Y/N
257	04231716+2757432	65.821480	27.962071	1417 ± 1307	-6.5 ± 4.3	-9.1 ± 4.3	34.9 ± 1.9	B9	Y:	N/N
258	04233427+2947149	65.892807	29.787510	6340 ± 1232	-1.5 ± 4.3	-5.6 ± 4.3	12.7 ± 1.4	A0	N	N/Y
259	04233438+3056585	65.893272	30.949650	3320 ± 420	4.8 ± 4.3	1.4 ± 4.3	-20.8 ± 1.8	A0	N	N/N
260	04234983+2532157	65.957558	25.537720	11883 ± 2984	2.2 ± 4.2	-1.7 ± 4.2	49.3 ± 3.2	A0	N	N/N
261	04240540+2744507	66.022369	27.747620		-0.3 ± 4.3	-5.5 ± 4.3	53.3 ± 2.8		?	N/N
262	04240902+2611351	66.037521	26.193510		4.2 ± 3.9	-4.8 ± 3.9	-17.2 ± 5	0	?	N/N
263	04243937+2946563	66.164047	29.782440	12882 ± 4098	3.2 ± 4.8	-5.9 ± 4.8	12.9 ± 2.4	A0	N	N/Y
264	04244689+2826203	66.195351	28.439030	16870 ± 6801	0.7 ± 4.9	-4.7 ± 4.9	12.1 ± 2.3	A0	N	N/Y
266	04245454+3014488	66.227280	30.246929	9024 ± 2583	-1.4 ± 4.3	-1.6 ± 4.3	-20.4 ± 2	A0	N	N/N
267	04254650+2805257	66.443710	28.090530	10098 ± 1561	-2.5 ± 4.4	-4.9 ± 4.4	29.9 ± 4.2	B9	N	N/N
268	04254749+3039409	66.447868	30.661350	10176 ± 3362	-3.3 ± 4.4	-6.1 ± 4.4	2.8 ± 2.6	A0	N	N/N
269	04255111+3041231	66.462982	30.689720	5837 ± 1217	-6.7 ± 4.3	-1.8 ± 4.3	41.9 ± 2.5	A0	N	N/N
270	04262320+2629082	66.596626	26.486160		-1.4 ± 3.9	-3.8 ± 3.9	15.9 ± 12.6	0	?	N/Y
271	04263605+2904190	66.650147	29.072081	5375 ± 1263	-2.2 ± 4.3	-2.2 ± 4.3	-16.1 ± 1.4	A0	N	N/N
272	04263695+3035247	66.654030	30.590200	9300 ± 1949	-4.4 ± 4.2	-3.0 ± 4.2	7.2 ± 2.8	A0	N	N/N
273	04264332+3054283	66.680603	30.907900	6815 ± 1694	-2.3 ± 4.1	1.2 ± 4.1	18.7 ± 1.9	A0	N	N/Y
274	04265712+2920054	66.737999	29.334990	4125 ± 496	0.0 ± 4.3	-8.3 ± 4.3	3.2 ± 1.4	A0	N	N/N
275	04300090+2511506	67.503799	25.197390	11767 ± 4813	-0.1 ± 3.9	-2.1 ± 3.9	11.1 ± 3.1	A0	N	N/Y
276	04304916+2527382	67.704887	25.460671	11299 ± 2639	0.4 ± 4.3	-3.1 ± 4.3	30.3 ± 3.2	A0	N	N/N
277	04324026+2537105	68.167717	25.619631	9909 ± 1761	2.9 ± 4.2	-2.5 ± 4.2	92.8 ± 3.8	A0	N	N/N
278	04325041+2613573	68.210083	26.232540		1.8 ± 3.8	-8.8 ± 3.8	-33.1 ± 7		?	N/N
279	04343357+2538478	68.639870	25.646650		0.7 ± 3.8	-11.1 ± 3.8	41.1 ± 4.9		?	Y/N
280	04344093+2526178	68.670540	25.438280	9457 ± 2601	-0.2 ± 3.9	-0.9 ± 3.9	13 ± 3.3	A0	N	N/Y
281	04352460+2511584	68.852524	25.199591		0.6 ± 3.9	-0.4 ± 3.9	1.3 ± 3.4		?	N/N
282	04352506+2505371	68.854431	25.093679	8742 ± 1788	1.9 ± 4.0	-1.8 ± 4	9.5 ± 3.8	A0	N	N/Y
283	04355804+2429239	68.991859	24.490030	4305 ± 611	-2.0 ± 3.7	-2.1 ± 3.7	39.6 ± 2.3	A0	N	N/N
284	04360432+2512256	69.018021	25.207150	7098 ± 1703	3.5 ± 3.7	-0.5 ± 3.7	83.4 ± 4	A0	N	N/N
285	04364715+2508462	69.196533	25.146160	7047 ± 1224	-1.4 ± 3.9	-0.6 ± 3.9	21.8 ± 3.1	A0	N	N/N
286	04374665+2415466	69.444412	24.262991	8970 ± 2523	-3.6 ± 3.9	-3.3 ± 3.9	-24.1 ± 2.9	A0	N	N/N
287	04384454+2438388	69.685593	24.644190		-0.3 ± 3.8	-5.4 ± 3.8	16 ± 3.6		?	N/Y
288	04384756+2524115	69.698174	25.403200		1.4 ± 3.8	-3.1 ± 3.8	34.2 ± 6.9		?	N/N
289	04391699+2520299	69.820900	25.341660		-6.7 ± 3.8	2.0 ± 3.8	30.2 ± 7.7		?	N/N
290	04393029+2457401	69.876183	24.961180		17.8 ± 3.8	-2.4 ± 3.8	11.9 ± 2.5		?	N/Y
291	04400871+2451438	70.036377	24.862181		0.9 ± 3.8	2.5 ± 3.8	28.1 ± 5		?	N/N
292	04402154+2629461	70.089851	26.496161		-3.5 ± 3.8	-6.1 ± 3.8	-21.3 ± 4.2		?	N/N
293	04402572+2635205	70.107269	26.589060		-6.6 ± 3.8	5.4 ± 3.8	-26 ± 5.4		?	N/N
294	04415750+2451568	70.489609	24.865770		-0.1 ± 4.0	1.5 ± 4	66.5 ± 3.5		?	N/N
295	04422622+2459000	70.609337	24.983379		9.5 ± 4.0	-7.6 ± 4	22.7 ± 4.2		?	N/N
296	04422916+2422346	70.621521	24.376360		2.6 ± 4.2	-4.8 ± 4.2	3.9 ± 1.9		?	N/N
297	04423176+2601455	70.632378	26.029329		2.1 ± 4.0	-5.7 ± 4	2.5 ± 2.6		?	N/N
298	04435975+2529297	70.998970	25.491650		-1.3 ± 4.3	-5.1 ± 4.3	1.5 ± 3.2		?	N/N
299	04441407+2415542	71.058632	24.265110	12108 ± 5721	3.2 ± 4.2	-3.8 ± 4.2	31.7 ± 3	B9	N	N/N
300	04442409+2609464	71.100418	26.162939	14445 ± 5743	-3.0 ± 4.7	-7.9 ± 4.7	6.8 ± 2.7	A0	N	Y/N
301	04443402+2537401	71.141808	25.627850		-2.0 ± 4.3	-9.5 ± 4.3	54.6 ± 3.9		?	Y/N
302	04445791+2601458	71.241364	26.029421	4464 ± 486	-2.1 ± 4.3	-5.3 ± 4.3	51.3 ± 1.8	A0	N	N/N
303	04450067+2619327	71.252762	26.325800	9289 ± 1437	-0.1 ± 4.7	-7.3 ± 4.7	-17.3 ± 4	A0	N	Y/N
304	04452569+2417505	71.357018	24.297430	11112 ± 3705	1.4 ± 4.4	-7.1 ± 4.4	24.1 ± 3.2	A0	N	Y/N
305	04453199+2548133	71.383301	25.803770		-2.2 ± 4.3	-7.7 ± 4.3	89.7 ± 2.8		?	N/N
306	04461962+2434148	71.581787	24.570881		1.3 ± 4.3	-4.1 ± 4.3	-23.5 ± 5		?	N/N
307	04463405+2413551	71.641983	24.232010	11533 ± 1056	9.7 ± 4.9	1.3 ± 4.9	22.3 ± 3.4	B9	N	N/N
308	04464411+2620004	71.683830	26.333450	3561 ± 2188	-6.0 ± 4.4	-2.3 ± 4.4	-7.9 ± 2.6	A0	N	N/N
309	04464556+2550507	71.689850	25.847441		-4.6 ± 4.3	-9.0 ± 4.3	8.5 ± 2.5		?	N/Y
310	04464746+2419597	71.697853	24.333281	6966 ± 1113	-2.5 ± 4.4	-2.8 ± 4.4	20.5 ± 2.6	A0	N	N/Y

Table 3

List of candidate early-type stars. The table is divided into sections, each compiled from a different selection source, as described in the text. The last three columns state whether or not (Y/N) the star is a probable Taurus member based on two distance estimates (d), proper motion (μ), and radial velocity(RV); see text. Error on $d_{\rm SPEC}$ is the standard deviation of distances calculated here using B,V,R,J,H, and K magnitudes.

311	04464757+2448496	71.698288	24.813789			-3.2 ± 4.3	-2.6 ± 4.3	50.7 ± 2.5		?	N/N
312	04471316+2452301	71.804802	24.875071			9.5 ± 4.4	-13.3 ± 4.4	-25.5 ± 4.6		?	Y/N
313	04475295+2407358	71.970642	24.126699		14372 ± 3532	3.1 ± 4.8	-2.0 ± 4.8	14.1 ± 2.8	B9	N	N/Y
314	04481479+2412522	72.061668	24.214569		12093 ± 1796	0.2 ± 5.1	-6.6 ± 5.1	-24.5 ± 2.6	A0	N	Y/N
315	04484223+2405315	72.175957	24.092159		5295 ± 1494	3.4 ± 4.3	-8.7 ± 4.3	25.2 ± 2.3	B9	N	Y/N
316	04485467+2603349	72.227799	26.059731			3.8 ± 4.3	-8.2 ± 4.3	-15.3 ± 2.3		?	Y/N
317	04490164+2603474	72.256897	26.063191			-2.1 ± 4.3	-4.7 ± 4.3	-8.1 ± 3.1		?	N/N
318	04495186+2546445	72.466042	25.779091		4478 ± 1063	-1.4 ± 4.3	-4.7 ± 4.3	18 ± 2.2	B9	N	N/Y
319	04501677+2455582	72.569870	24.932921			7.7 ± 4.3	-14.6 ± 4.3	205.7 ± 3.1		?	Y/N
320	04502462+2534113	72.602654	25.569889			-0.1 ± 4.3	-12.8 ± 4.3	39.3 ± 4.2		?	Y/N
321	04502592+2609475	72.607941	26.163250			-0.5 ± 4.3	-9.7 ± 4.3	-8.8 ± 1.7		?	Y/N
322	04503511+2516324	72.646263	25.275740			5.1 ± 4.4	-5.4 ± 4.4	2.4 ± 4.3		?	N/N
323	04505387+2426576	72.724533	24.449440		7078 ± 1947	-1.5 ± 4.3	-3.9 ± 4.3	28.7 ± 2.2	A0	N	N/N
324	04511381+2522599	72.807442	25.383381		6538 ± 1250	5.6 ± 4.3	-4.0 ± 4.3	12.4 ± 2.5	B9	N	N/Y
325	04513070+2438129	72.877831	24.636990		3468 ± 296	10.7 ± 4.3	-7.0 ± 4.3	32 ± 2.5	A0	N	N/N
326	04521892+2520501	73.078812	25.347281		5194 ± 884	4.8 ± 4.3	-3.0 ± 4.3	63.8 ± 2	A0	N	N/N
327	04522135+2506498	73.088966	25.113840		9897 ± 2710	4.1 ± 4.4	-4.8 ± 4.4	26.4 ± 3.6	A0	N	N/N
					Other stars						
328	HD 31305	73.950958	30.337911		174 ± 11	6.4 ± 1.7	-21.9 ± 1.6		A1V	N	Y/?
329	HD 31293	73.941022	30.551191	139^{+22}_{-16}	121 ± 50	1.9 ± 0.9	-24.4 ± 0.7	8.9 ± 0.9	$\sim$A0V	Y	Y/Y

Table 4
Spectral types derived through new spectroscopy.

B#	Star		Equivalent Widths															Derived
		$\frac{SNR}{100}$	Ca II K 3933.7	N II 3995.0	He I 4009.3	He I 4026.2	H_δ 4101.7	He I 4120.8	Si II 4128.1, 4130.9	He I 4143.7	H_γ 4340.4	He I 4387.9	He I 4471.5	MgII 4481.2	H_β 4862.3	He I 4921.9	H_α 6562.8	He I 6678.2	SpT
							Spectral Type Standards												
	HD 36960	3.0	0.12	0.09	0.42	1.2	4.0	0.48	0.02	0.55	4.2	0.58	0.98	0.15	3.6	0.78	3.4	0.68	B0.5V
	HD 19374	2.6	0.15	0.08	0.56	1.5	5.7	0.35	0.08	0.82	5.2	0.87	1.6	0.20	5.4	0.97	4.2	0.66	B1.5V
	HD 35912	3.2	0.14	0.04	0.65	1.5	5.9	0.26	0.12	0.81	5.9	0.91	1.6	0.25	5.9	0.88	4.4	0.56	B2V
	HD 28375	2.6	0.13	0.01	0.30	1.1	7.6	0.20	0.21	0.45	7.6	0.61	1.1	0.28	7.4	0.56	5.5	0.31	B3V
	HD 16219	2.7	0.13	0.01	0.19	0.82	8.1	0.13	0.26	0.33	8.0	0.48	0.85	0.32	8.0	0.43	5.7	0.21	B5V
	HD 21071	2.7	0.14	<0.01	0.15	0.84	8.4	0.11	0.24	0.29	8.4	0.44	0.80	0.30	8.7	0.41	5.8	0.20	B7V
	HD 14272	1.7	0.19		<0.02	0.40	10.2	[a]	0.24	0.11	9.3	0.11	0.25	0.31	10.1	0.28	6.4	0.12	B8V
	HD 16350	1.9	0.57			[a]	12.3	[a]	0.26	0.08	17.8	[a]	0.10	0.38	11.9	<0.23	8.7	0.04	B9.5V
	HD 14171	1.7	0.29				14.6	[a]	0.30	[a]	13.0		0.023	0.33	13.6	[a]	9.4	[a]	B9.5V
							O,B stars listed in SIMBAD												
50	HD 283809	1.8	0.24	0.09	0.70	1.4	4.9	0.35	0.10	0.86	4.9	0.90	1.4	0.27	5.0	0.93	3.8	0.64	B1.5-2V
51	τ Tau	2.4	0.29	0.01	0.43	1.2	8.2	0.21	0.15	0.56	7.9	0.72	1.0	0.27	7.8	0.68	5.6	0.38	B3V
25	72 Tau	3.1	0.12	0.02	0.16	0.82	9.8	>0.1	0.24	0.27	9.2	0.49	0.75	0.31	8.6	0.41	6.0	0.18	B7V
88	HD 31806	3.4	0.12	0.01	0.21	0.77	9.7	[a]	0.22	0.27	8.7	0.45	0.72	0.34	8.8	0.39	6.4	0.19	B7V
6	HD 283304	1.2	0.42		0.03	[a]	8.9	[a]	0.79	[c]	8.2	0.15	0.07	0.16	8.2	0.20	6.6	<0.05	B8V Si
33	HD 282276	1.4	0.28	0.02	0.05	0.31	8.9	[c]	0.41	0.09	8.2	[a]	0.29	0.26	8.0	0.24	6.5	0.12	B8V
36	HR 1445	2.3	0.19	[c]	0.04	0.41	9.6	[a]	0.30	0.13	9.1	<0.20	0.32	0.32	8.7	0.26	6.7	0.05	B8V
13	V1137 Tau	2.9	0.18	0.01	0.11	0.29	6.4	>0.05	0.37	0.11	5.9	<0.22	0.30	0.22	6.5	0.22	5.9	0.09	B8III
48	HD 29647	1.6	0.31	0.04	<0.1	0.24	8.7	[a]	0.34	0.09	7.8	<0.19	0.26	0.39	7.7	0.22	6.1	0.06	B9III
81	HD 283971	1.6	0.92	0.01	0.03	0.25	11.1	[a]	0.25	0.07	9.5	[a]	0.19	0.38	10.6	<0.22	7.9	<0.05	B9V
63	HD 30378	3.0	0.28	<0.01	0.01	0.24	13.6	[a]	0.24	0.06	13.0	<0.1	0.27	0.44	12.7	0.18	9.1	<0.05	B9.5V
4	BD+23607	2.3	1.1	<0.01	[c]	<0.01	16.6	[a]	[a]	[a]	14.0	[a]	0.08	0.38	13.9	<0.19	9.7	<0.02	A0V
12	HD 283449	1.2	0.75	[c]	[c]	0.23	14.3	[a]	0.26	<0.09	13.7	[c]	0.11	0.46	14.3	0.14	10.7	<0.05	A0V
53	V1081 Tau	3.1	0.59	[a,c]	[c]	0.11	16.8	[a]	[a]	0.01	16.8	[a]	0.13	0.37	15.8	<0.16	10.7	<0.03	A0V
19	V892 Tau	0.5	[a]		[c]	∼0.17	∼14.0	[c]	[c]	[c]	[b]	[c]	[c]	∼0.16	[b]	[c]	[b]	[c]	∼A0Ve
							Early-type stars from Rebull et al. (2010)												
95	HD 283751	1.5	0.39	0.49	0.26	0.82	8.0	0.13	0.23	0.36	[b]	0.50	0.79	0.32	[b]	0.31	[b]	0.21	B5Ve
90	HD 27923	2.3	0.24	[c]	0.04	0.33	12.9	[a]	0.18	0.07	11.8	<0.21	0.27	0.35	11.5	0.18	8.2	<0.05	B9V
91	HD 283637	1.6	0.91	[c]	∼0.05	<0.32	15.9	[a]	>0.04	[a,c]	13.7	[a]	∼0.11	0.37	13.6	0.22	[b]	0.1	B9.5eV
94	HD 284530	2.1	0.34	<0.01	[c]	0.30	13.6	[a]	0.30	0.09	11.7	<0.35	0.25	0.38	11.5	0.24	8.5	<0.07	B9.5V
93	2MASS0431+29	1.9	0.48		<0.03	[a]	16.6	[a]	[a]	[c]	17.2	[a/c]	<0.06	0.27	15.6	<0.24	10.9	<0.01	A1V
89	HD 27659	1.0	2.6		<0.19	⩽0.16	10.4	[a]	∼0.37	⩽0.19	10.4	<0.39	<0.23	0.47	11.6	<0.48	10.1	∼0.1	A3V
92	2MASS0428+27	0.3	∼3.5	[a]	<0.04	[c]	∼12	[a]	∼0.5	<0.2	∼12	[a]	<0.6	0.87	∼14	<0.11	9.6	0.14	A4III
							O,B stars selected using 2MASS colors												
106	HD 26212	1.2	3.9	[a]	[a]	[a]	11.8	[a]	∼0.35	⩽0.16	8.9	<0.33	<0.21	0.41	9.0	⩽0.42	9.6	∼0.1	A5V
							Other												
328	HD 31305	1.8	1.7		[c]	<0.27	17.6	[a]	∼0.28	<0.09	16.3	<0.28	<0.16	0.46	15.0	<0.27	9.6	<0.02	A1V
329	AB Aur	2.4	[b]						∼0.17					0.40			[b]	[b]	A0Ve

B# is repeated from Table 3. SNR is the signal-to-noise ratio of the obtained spectrum. Notes- (a) embedded in an adjacent absorption line, (b) emission line present within the absorption line, (c) hard to distinguish from noise.

Table 5
Physical parameters derived through model atmosphere fitting.

Star	$T_{\rm eff}$ (K)	$v \cdot \sin i$ (km s^{-1})	log g (cgs)	SpT
HD 283809	21000	< 50	4.0	B2V
HD 29763 = τ Tau	18000	150	4.0	B3V
HD 283751	15000	50	4.0	B5V
HD 28149 = 72 Tau	14000	75	4.0	B7V
HD 31806	14000	100	4.0	B7V
HD 28929 = HR 1445	13000	< 50	4.0	B7V
HD 26571 = V1137 Tau	13000	< 50	3.5	B7III
HD 284530	12000	< 50	4.0	B7.5V
HD 283971	12000	50	4.0	B7.5V
HD 283304	12000	< 50	3.5	B8III
HD 282276	12000	< 50	3.5	B8III
HD 29647	11500	< 50	3.5	B8III
HD 27923	11000	< 50	4.0	B8.5V
AB Aur	11000	200	4.5	B8.5V
2MASS J04313313+2928565	11000	250	4.5	B8.5V
HD 31305	11000	150	4.5	B8.5V
HD 30378	11000	< 50	4.0	B8.5V
V892 Tau	11000	100	4.5	B8.5V
HD 29935 = V1081 Tau	11000	200	4.5	B8.5V
HD 283637	11000	50	4.0	B8.5V
BD+23 607	10000	< 50	4.0	A0V
HD 283449	10000	< 50	4.0	A0V
HD 27659	9000	< 50	3.5	A1III
2MASS J04285940+2736254	9000	< 50	3.5	A4III
HD 26212	8500	< 50	3.5	A5III

Table 6
Final list of early-type stars showing indications of membership with Taurus.

B#	HD Number	Alt. Identifier	$\alpha_{\rm J2000}$ (h,m,s)	$\delta_{\rm J2000}$ ($^\circ$,$'$,$''$)	SpT	d_{HIP} (pc)	d_{SPEC} (pc)	$P(\chi^2)$ (%)	RV (km s^{-1})	Comments
Probable members based on our analysis of distance and/or kinematics										
51	HD 29763	τ Tau	04 42 14.70	22 57 24.9	B3V	123^{+13}_{-11}	137 ± 9	5.1	12.3 ± 4.1	
25	HD 28149	72 Tau	04 27 17.45	22 59 46.8	B7V	127^{+13}_{-11}	161 ± 3	2.4	7.3 ± 2.6	IR nebula; cool dust SED
36	HD 28929	HR 1445	04 34 37.99	28 57 40.1	B8V	143^{+20}_{-16}	157 ± 3	11.5	12.6 ± 2.2	Weak nebula
19	—-	V892 Tau	04 18 40.62	28 19 15.5	$\sim$B8.5–A0Ve		†	25.7		IR nebula; Class I SED
329	HD 31293	AB Aur	04 55 45.85	30 33 04.3	A0Ve	139^{+22}_{-16}	120 ± 50	36.1	8.9 ± 0.9	Class II type SED
328	HD 31305	IRAS 04526+3015	04 55 48.23	30 20 16.5	A1V		174 ± 11	21.5		Cool dust SED
193	HD 31648	MWC 480	04 58 46.27	29 50 37.0	A3Ve	137^{+31}_{-21}	186 ± 48	18.8		Class II type SED
106	HD 26212	—-	04 09 43.68	24 04 22.6	A5V	123^{+17}_{-14}		3.3	20.3 ± 3.9	
Candidates with several membership indicators but that are not secure distance and kinematic members										
46	—-	IC 2087	04 39 55.75	25 45 02.0	B5:			46.7		IR+visible nebula; Class I type SED
96	HD 283815	—-	04 42 41.18	24 41 17.9	A0		268 ± 40	12.8		Meets proper motion but not distance criteria
89	HD 27659	—-	04 22 54.66	28 23 55.0	A3V		164 ± 10	< 0.1		Meets distance but not proper motion criteria; cool dust SED
Stars illuminating infrared nebulae but that can not be associated with Taurus based on distance and kinematic criteria										
33	HD 282276	—-	04 33 04.23	29 21 49.9	B8V		422 ± 52	< 0.1		IR nebula; cool dust SED; NOTE: $P(\chi^2) = 6.2$ for Taurus grp. V
48	HD 29647	IRAS 04380+2553	04 41 08.05	25 59 34.0	B9III	177^{+43}_{-29}	160 ± 1	< 0.1		IR nebula; cool dust SED

(1) B# is repeated from Table 3. (2) SpT is the spectral type as revised in this work or from literature. (3) The probability of proper motion membership, $P(\chi^2)$, is as discussed in Section 2.3.2. (4) The membership criteria used in this work are: $P(\chi^2) > 1\%$, $128 < d < 162$ pc within 1σ error, and $9.8 \leq RV \leq 17.5$ km s^{-1} wherever radial velocity is available. † $d_{SPEC} = 1697 \pm 1548$ pc, $d_B = 4720$ pc, $d_K = 135$ pc